



Review Article

A review of Whipple shield ballistic limit equations

S Ryan^{a,*}, WP Schonberg^b^a Applied Artificial Intelligence Institute, Deakin University, Wauurn Ponds, VIC 3216, Australia^b Civil, Architectural, and Environmental Engineering Department, Missouri University of Science and Technology, Rolla, MO 65409, USA

ARTICLE INFO

Keywords:

Hypervelocity impact
Space debris
Whipple shield
Ballistic limit

ABSTRACT

Ballistic limit equations (BLEs) are semi-analytical expressions used to predict the risk posed by micrometeoroid and orbital debris (MMOD) impacts on a spacecraft. A foundational BLE, known as the new non-optimum (NNO) equation was published by Eric Christiansen of NASA Johnson Space Center in 1990 for application on Whipple shields – two-plate configurations consisting of a thin sacrificial plate located at some standoff in front of the spacecraft pressure hull or structural wall. Today, BLEs for almost all multi-plate spacecraft structures, e.g., honeycomb sandwich panels, monolithic structures with thermal insulation blankets, etc., are based on the NNO Whipple BLE. We review the development of the NNO BLE as well as some prominent modifications and evaluate their performance against collated databases of hypervelocity impact experiments. Finally, a further modification to the NNO BLE is proposed that allows for extension to Whipple shields with under-sized bumper plates without the computational inconsistencies of the current state-of-the-art methodology.

1. Introduction

In 1947 astronomer Fred L. Whipple proposed the use of a ‘meteor bumper’, consisting of a thin sheet of metal placed at a small distance in front of a spacecraft hull [1]. This bumper would induce an explosion of the impacting meteorite, leading to its vaporisation and the dissipation of its impact energy when impacting upon the spacecraft hull (i.e., reduced penetration capability). This process is schematically depicted in Fig. 1. The disrupted projectile and bumper material form a cloud of solid, molten, and/or vapourised debris which expands radially as it propagates towards the rear wall, leading to impact over a dispersed area. A two-wall structure for protecting against micrometeoroid and orbital debris (MMOD) particle impacts, such as that seen in Fig. 1, is named in honour of Dr Whipple – the Whipple shield.

The behaviour of MMOD particles upon impact with a thin bumper plate, and subsequently the protective performance of a Whipple shield, varies with the velocity of the impacting particle. Penetration behaviour can be separated into three distinct phenomenological regions (see e.g., [3]):

1. Low speed impacts, where the projectile may be deformed and/or eroded by its passage through the bumper plate but isn't fragmented. Thus, penetration of the rear wall is by a single projectile fragment with speed equal to or less than the impacting projectile.

2. Intermediate speed impacts, where the penetration transitions between a low speed and high-speed impact in a complicated way because of projectile fragmentation and melting.
3. High-speed impacts where the projectile and holed-out bumper plate material are completely, or nearly completely, melted and/or vaporized by the impact. The resulting cloud of debris impulsively loads the rear wall, resulting in rupture and petalling type failure (complete perforation) or detached spallation from the rear surface of the rear wall.

Whipple shields are uniquely important in MMOD shielding as almost all shields, either dedicated or dual-purpose, are based on the Whipple concept – namely, a multi-wall structure of which the outer plate(s) is/are intended to induce a disruption of the impacting MMOD particle such that the energy of the particle is dispersed over a larger area of the rear wall (or spacecraft pressure hull). This commonality is demonstrated in Fig. 2.

The performance of spacecraft structures under hypervelocity impact of MMOD particles can be approximately described by simple analytical expressions, referred to as Ballistic limit equations (BLEs). Typically, BLEs are based on analytical considerations, e.g., conservation of momentum, conservation of energy, etc., with empirical adjustments to improve agreement with experimental data. BLEs are commonly used to (1) size spacecraft structural elements or dedicated shields to provide

* Corresponding author.

E-mail address: shannon.ryan@deakin.edu.au (S. Ryan).

physical protection against the MMOD environment, and (2) predict the risk posed by the MMOD environment to a spacecraft mission or critical element (e.g., failure of a fuel tank, astronaut loss of life, etc.). BLEs for almost all MMOD shields, either dedicated or dual-purpose, are based on pioneering forms of that derived for Whipple shields for Space Station Freedom [4]. Thus, in understanding and evaluating multi-plate MMOD shields and their respective BLEs it is important to understand the history of the Whipple shield BLE, its derivation, experimental validation, and shortcomings.

This review addresses the Whipple shield BLE, specifically its genesis during Project Apollo, its ongoing development for the Space Station Freedom (SSF), Shuttle Orbiter, and International Space Station programs, and some key modifications proposed over the past two decades. This review is not an exhaustive survey of all Whipple shield BLEs available in the open literature, but instead focused on several key variants – an overview of which is provided in Table 1.

2. Background

The first BLEs for Whipple shields were developed during Project Apollo for sizing structural walls of the Command Module and Lunar Lander to protect against micrometeoroid impacts [6]. The General Motors Defense Research Laboratories (GMDRL) developed sizing equations for Whipple shield rear walls under ‘optimal’ conditions – where the debris cloud, following impact with the bumper, is entirely molten and/or vaporised and loading of the rear wall is impulsive in nature. Given impact conditions and a suitably sized bumper plate suitable for generating such an optimum debris cloud, the required rear wall thickness of a Whipple shield to prevent failure was calculated by Maiden et al. [5]:

$$t_w = \frac{C m_p V}{S^2} \quad (1)$$

where t_w is the rear wall thickness in mm, m_p is the projectile mass in grams, S is the standoff between the bumper plate and rear wall in cm, V is the impact velocity in km/s, and C is an empirical constant equal to 415 ± 140 for AA7075-T6 rear walls with an assumed failure mode of rear wall yielding.

In practise it is difficult to always ensure optimum debris cloud conditions. As such, a more conservative approach which assumed the

presence of solid projectile/bumper fragments in the debris cloud that lead to cratering type failure of the rear wall was developed by Cour-Palais in [6] for application on Whipple shields under non-optimum conditions:

$$t_w = \frac{C m_p^{1/3} V}{S^{1/2}} \quad (2)$$

where $C = 0.055(\rho_p \rho_b)^{1/6}$ is an empirical constant that allows the equation to be applied to projectile and bumper materials other than glass on AA2024-T3, for which the equation was originally developed.

Whereas the required rear wall thickness for the optimum condition scales with projectile momentum ($t_w \propto m_p V$) and is inversely proportional to the square of standoff, S , in the non-optimum condition the rear wall thickness scales with the cube root of projectile kinetic energy, ($t_w \propto KE^{1/3} \propto d_p \rho_p^{1/3} V^{2/3}$ [4]) and an inverse square root dependence on spacing, S . Kinetic energy scaling is a conservative approach consistent with NASA guidelines from 1970 for extrapolating to impact velocities beyond the capabilities of laboratory accelerators [12]. The inverse square root dependence of rear wall sizing on shield spacing was based on empirical evidence [13].

3. A three-part ballistic limit equation for Whipple shields

Following Project Apollo, the impact protection design requirements for Skylab and the Space Shuttle program were based on the natural meteoroid environment. The Space Station Freedom (SSF) program was the first to specify a protection requirement that considered the man-made orbital debris environment [14].

In the mid-1980s, Boeing, under contract to the NASA Marshall Space Flight Center, developed the BUMPER computer program for calculating the risk posed to a spacecraft from impact of micrometeoroids or orbital debris [7]. The so-called ‘response’ equations used in BUMPER defined a three-part curve with mechanism-specific sections of the curve corresponding to the low, intermediate, and hypervelocity regimes phenomenologically described in [3]. In the low velocity regime, the PEN4 software package was used [15], while the hypervelocity regime adopted the Wilkinson equation [16]. In the intermediate regime a multi-variate regression was fit to newly generated test data. To identify the low-to-intermediate transition velocity the critical projectile diameter was calculated using both the PEN4 and multi-variation

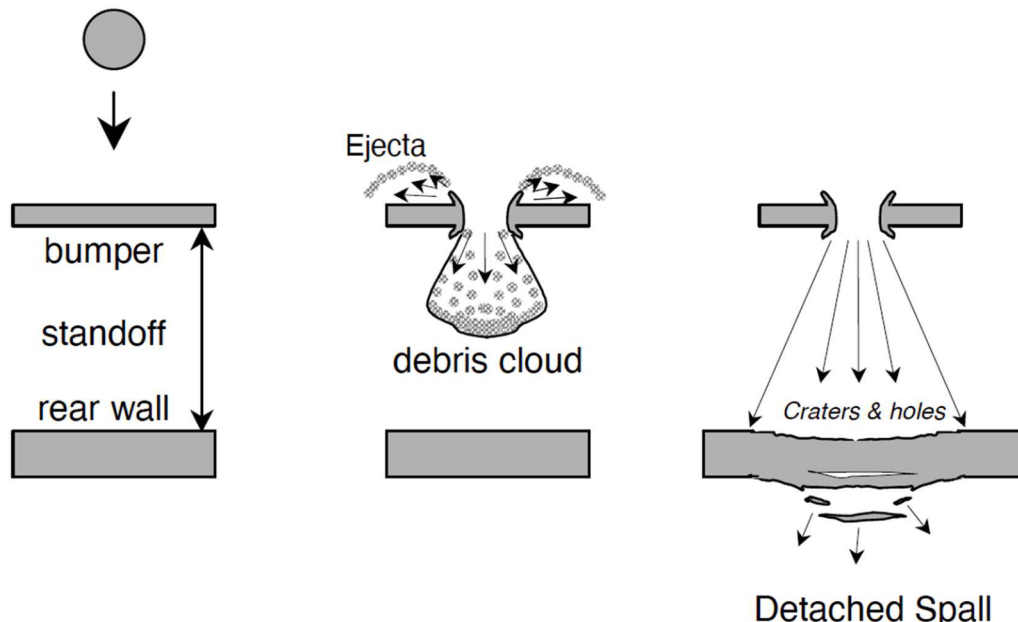


Fig. 1. Concept of a ‘Whipple shield’ for hypervelocity impact protection of spacecraft, from [2].

regression models. The velocity where the critical diameter calculated by the regression model exceeds that of the PEN4 model is used to indicate the regime transition [7,17]. Similarly, the intermediate-to-hypervelocity regime transition is identified as the velocity at which the Wilkinson predictor calculates a smaller critical projectile velocity than the regression model [7,17]. An example of the resulting ‘response’ curve, expressed in terms of the critical projectile diameter above which a defined Whipple shield rear wall will be perforated, is plotted in Fig. 3.

4. New non-optimum BLE

In the late 1980s and early 1990s NASA performed additional work on Whipple shields [18] and, with configuration control for BUMPER coming under Johnson Space Center, three-part ballistic limit ‘response’ equations become the standard. In [4], and then publicly in [19], Christiansen presented an alternate set of equations for sizing or determining the performance of Whipple shields, drawing on Cour-Palais’ research during the Apollo program. This set of equations is commonly referred to as the “new non-optimum” or NNO BLE. The non-optimum equation for sizing a Whipple shield rear wall, Eq. (2), was valid for applications with projectile diameters between 0.08 and 0.16 cm and

shield spacing-to-projectile diameter ratios greater than 50, i.e., $S/d_p > 50$ [13]. Additional impact tests were performed on Whipple shields at or near the ballistic limit, covering a range of projectile diameters (0.04 cm–1.9 cm), projectile materials (Nylon, glass, Aluminum), impact velocities (6.7 km/s–7.5 km/s), bumper thickness-to-projectile diameter ratios (0.08–0.64), and shield spacing-to-projectile diameter ratios (13–96). All tests were performed at normal incidence. It was found that for larger projectiles, the non-optimum Whipple shield equation was non-conservative in that it was able to correctly predict only 70 % of the rear wall failures that new experiments had shown would result in rear wall failure [2], see Fig. 4 and Table 2.

Cour-Palais had derived new coefficients C for each of three different projectile diameter regimes, including the original Apollo data ($d_p = 0.08 – 0.16$ cm), $d_p = 0.32 – 1.0$ cm, and constant $d_p = 1.9$ cm [13]. Christiansen generalised the C coefficient by incorporating the square root of the projectile diameter, defining the NNO rear wall sizing equation (from [4]) as:

$$t_w = \frac{C d_p^{1/2} (\rho_p \rho_b)^{1/6} m_p^{1/3} V_n}{S^{1/2}} \left(\frac{70}{\sigma_y} \right)^{1/2} \quad (3)$$

where $C = 0.19$ (units $\text{cm}^2 \text{ sec/g}^{2/3} \text{ km}$) initially in [20] for aluminium-on-aluminium impacts and updated to 0.16 in [4], V_n is the

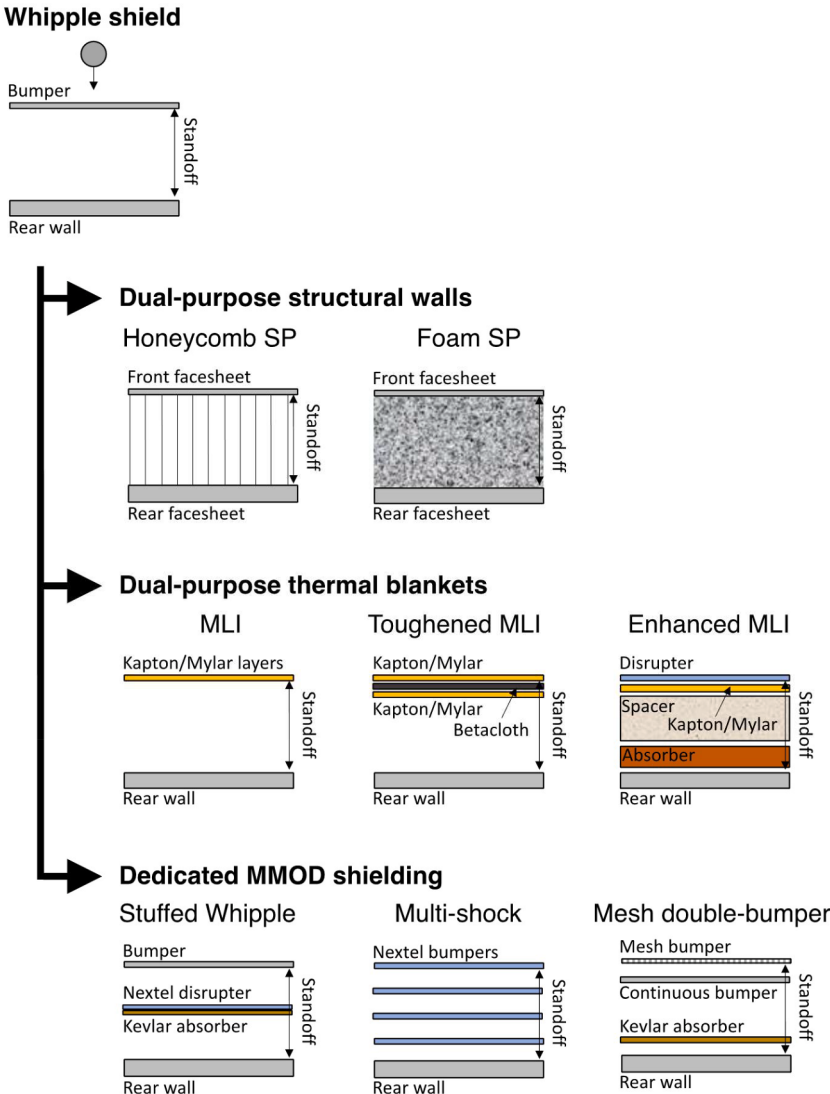
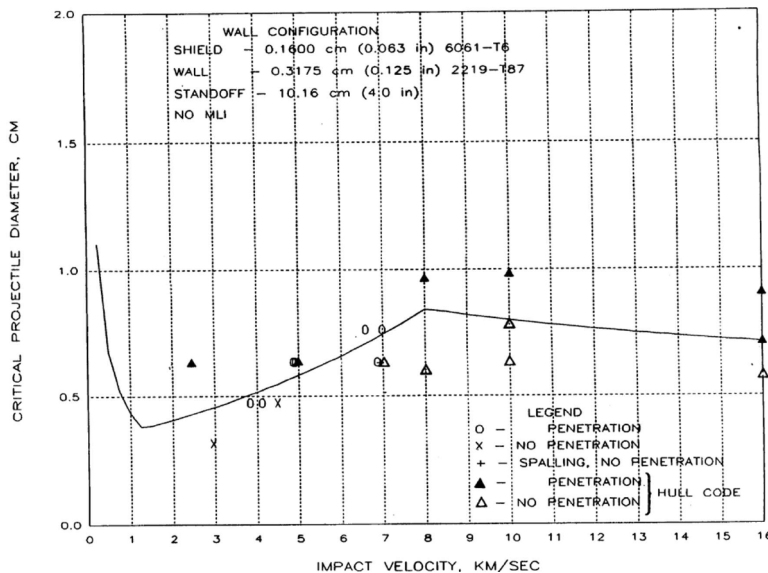


Fig. 2. Whipple shields are the common ancestor of almost all spacecraft MMOD shields, either dedicated, dual-purpose structural walls, or dual-purpose thermal blankets.

Table 1

Overview of the ballistic limit equations included in this review.

Equation name	Author(s)	Publication year	Reference	Main innovation	Experimental data
Optimum	CJ Maiden, AR McMillan, RE Sennett, JW Gehring	1965	[5]	First Whipple shield rear wall sizing equation, applicable for impact of micrometeoroids in “optimal” conditions (i.e., fully molten and/or vapourised debris cloud following impact with the shield outer wall)	Unknown (reference [5] lists 141 hypervelocity impact experiments with velocities between 0.72 – 8.08 km/s).
Non-optimum	B Cour-Palais	1969	[6]	Whipple shield rear wall sizing equation applicable for impact of micrometeoroids in “non-optimal” conditions (i.e., debris cloud containing some residual solid fragments following impact with the shield outer wall)	Unknown number of impact tests with aluminium and glass projectiles of diameters up to 0.16 cm. Impact velocities between 6.5 – 8 km/s.
BUMPER response equation	AR Coronado, MN Gibbins, MA Wright, PH Stern	1987	[7]	First three-part Whipple shield performance equation covering orbital debris-relevant impact velocities as well as micrometeoroids	Unknown
New non-optimum (NNO)	EL Christiansen	1991	[4]	Simplified closed-form analytical three-part Whipple shield sizing and performance equation	55 compiled hypervelocity impact experiments V: 5.88 – 8.06 km/s Data provided in [4]
Christiansen-modified NNO	EL Christiansen, JH Kerr	2001	[8]	Modification of the NNO in the hypervelocity regime to account for insufficiently thick bumper plates (i.e., those not sized according to the NNO requirement)	Approx. 200 compiled hypervelocity impact experiments V: 2 – >8 km/s Data not published
Reimerdes-modified NNO	HG Reimerdes, D Noelke, FK Schaefer	2006	[9]	Alternate modification of the NNO in the hypervelocity regime to account for insufficiently thick bumper plates (i.e., those not sized according to the NNO requirement); introduction of a bumper thickness-dependent projectile fragmentation velocity, and; utilisation of an alternate low velocity performance equation (Fish-Summers, compared to NNO’s use of the Cour-Palais cratering equation)	8 new hypervelocity impact experiments V: 2.57 – 7.17 km/s Data provided in [9]
JSC Whipple	S Ryan, EL Christiansen	2009	[10]	Modified NNO incorporating Reimerdes’ hypervelocity modification for undersized bumper plates and bumper thickness-dependent projectile fragmentation velocity.	444 compiled hypervelocity impact experiments V: 0.72 – 8.08 km/s Data provided in [11]
Modified JSC Whipple	S Ryan	2023	This article	Modifications to the Reimerdes’ hypervelocity de-rating factor for improved consistency and computational stability.	1135 compiled hypervelocity impact experiments V: 0.72 – 9.89 km/s Data provided in [11]

**Fig. 3.** Whipple shield ballistic limit response curve showing the three velocity regimes, calculated using BUMPER [7].

normal component of the velocity vector for oblique impacts, $V_n = V\cos\theta$, θ is the impact obliquity measured from the normal of the bumper surface, and $(\frac{\sigma_0}{\sigma_y})^{1/2}$ is a material correction factor from [6] that is required to associate the equation with the original experimental data on AA7075-T6 (where σ_y is the 0.2 % offset tensile yield strength of the rear wall material in ksi). Note that modifications to the equations from

previous forms are indicated in bold type (in Eq. (3) and throughout the remainder of this manuscript).

The NNO modifications improved the performance of the BLE against the new, large projectile dataset in [4], as shown in Fig. 5 and Table 2.

Sizing of the bumper plate was also modified,

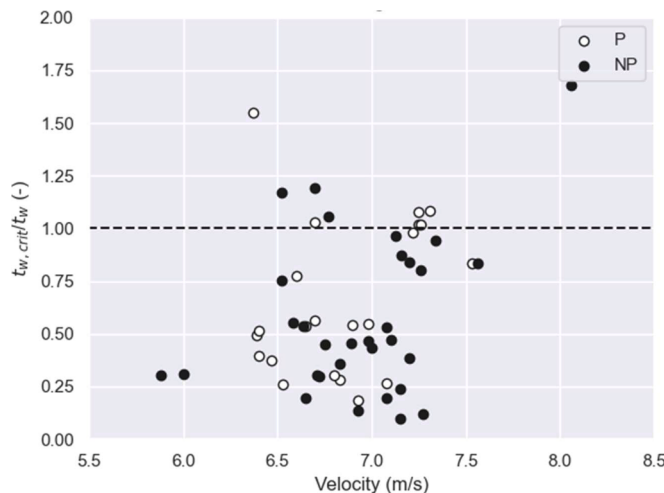


Fig. 4. Evaluation of the non-optimum BLE, Eq. (2), applied to hypervelocity impact test data from [4] that includes projectile diameters up to 1.9 cm.

$$t_b = \begin{cases} 0.25 d_p \rho_p / \rho_b & \text{for } S/d_p < 30 \\ 0.20 d_p \rho_p / \rho_b & \text{for } S/d_p \geq 30 \end{cases} \quad (4)$$

The constant, C , was increased from 0.20 [21] to 0.25 to reduce the possibility of underestimating the required rear wall thickness for Whipple shields with small standoff distances (i.e., when $S/d_p < 15$). The projectile-to-bumper material density ratio was introduced to prevent over-sizing of bumpers that were exposed only to low density meteoroid flux [4].

Expressed in terms of shield performance, the NNO is given as:

$$d_c = 3.918 \frac{t_w^{2/3} S^{1/3}}{(V \cos \theta)^{2/3} \rho_p^{1/3} \rho_b^{1/9}} \left(\frac{\sigma_y}{70} \right)^{1/3} \quad (5)$$

Eq. (5) is valid for impacts in which the normal component of the velocity vector, V_n , is 7 km/s or higher. This is often referred to as the “hypervelocity regime”, corresponding to a debris cloud that consists mostly of molten (or vapourised) material. Like Cour-Palais’ non-optimum assumption of residual solid fragments, sizing, and performance in the hypervelocity regime of the NNO equation is based on cratering-type failure from solid fragments; hence, the required rear wall thickness scales with impactor kinetic energy [22]. The 7 km/s transition velocity is based on experiments from [23], where the debris cloud for aluminium-on-aluminium impacts (assuming correctly sized bumper plates) were observed to consist of small molten particles or vapour for impacts above 7 km/s. This finding is in disagreement with 1D models from [24], which suggest aluminium projectiles should be completely molten after impacting on aluminium plates at impact velocities above 7–8 km/s. Hydrocode simulations presented in [25] identify that the 1D models fail to account for 3D free-surface effects which act to degrade the compressive shock wave in the projectile and, subsequently, reduce the degree of fragmentation/melt/vaporisation that occurs in comparison with that predicted by the 1D models.

At lower impact velocities the shock and release waves generated during impact are inadequate to induce projectile fragmentation. In [23] incomplete projectile fragmentation of the projectile was observed for aluminium-on-aluminium impacts at velocities below 7 km/s (for

correctly sized bumper plates), with solid fragments inflicting significant damage on the rear sheet. For a Whipple shield with a correctly sized bumper plate the thickness of a rear wall required to prevent perforation was experimentally observed in [5,23] to reach a maximum between approximately 2.5–3.5 km/s, see Fig. 6.

For impact velocities below this maximum the projectile passes through the bumper plate intact, albeit potentially deformed. Christiansen proposed an approach based on Cour-Palais’ cratering relationship for a finite shield, from [26]:

$$t_s = k \cdot 5.24 \cdot d_p^{19/18} \cdot H B_s^{-0.25} \left(\rho_p / \rho_s \right)^{1/2} (V/C_s)^{2/3} \quad (6)$$

for $0.5 \leq \rho_p < 2.78 \text{ g/cm}^3$,

where $H B_s$ is the hardness of the shield material in Brinell, C_s is the bulk soundspeed of the shield material in km/s, and k is an empirical constant related to the plate failure model equal to 3.0, 2.2, and 1.8 to prevent incipient spallation, detached spallation, and perforation, respectively. The 19/18 exponent in Cour-Palais’ original cratering equation is based on experimental findings at NASA’s Johnson Space Center and Ames Research Center [26]. In [27] Denardo et al. performed a series of cratering experiments with polyethylene and aluminium spheres. They found that the crater depth did not scale exactly with $V^{2/3}$, rather, there was a slight projectile size effect. By incorporating a moderate diameter dependence, $d_p^{19/18}$, the data collapsed much better on the $V^{2/3}$ curve.

For use in sizing Whipple shields in the low velocity regime, Christiansen proposed some modifications to Eq. (6),

- Increased angle dependence of the penetration depth from 2/3 to 5/3 to allow for the inclusion of slant range, which considers that at oblique angles of impact the penetration depth is measured along the flight vector rather than normal to the target surface, thus the relationship $t_w \propto k$ in the Cour-Palais cratering relationship is modified to $t_w \propto (k \cos \theta)$.
- Cour-Palais defines the semi-infinite plate material in terms of Brinell hardness (HB), soundspeed (C), and density (ρ). Christiansen replaced these properties with a single material coefficient of 0.6,

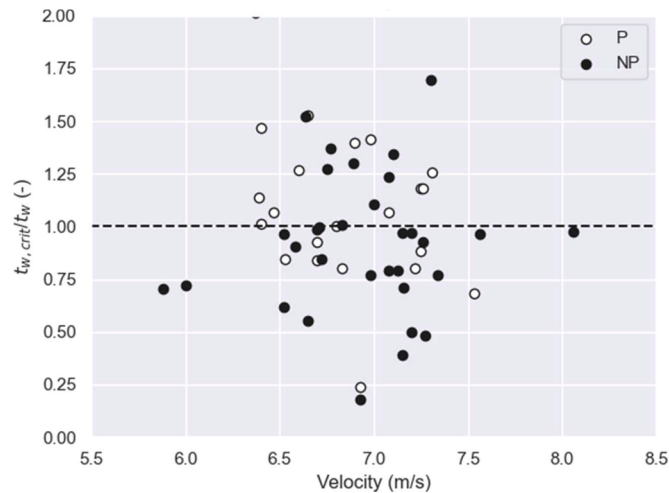


Fig. 5. Evaluation of the new non-optimum BLE, Eq. (2), applied to hypervelocity impact test data from [4] that includes projectile diameters up to 1.9 cm.

Table 2

Performance of the new non-optimum (NNO) sizing BLE, Eq. (3), applied to the database in [4], compared with Cour-Palais’ original non-optimum sizing BLE, Eq. (2).

Model	Accuracy		Precision	Recall	F1-score
	Overall	“P” class			
Non-optimum	0.618 (34/55)	0.304 (7/23)	0.844 (27/32)	0.58	0.30
NNO	0.691 (38/55)	0.652 (15/23)	0.719 (23/32)	0.65	0.64

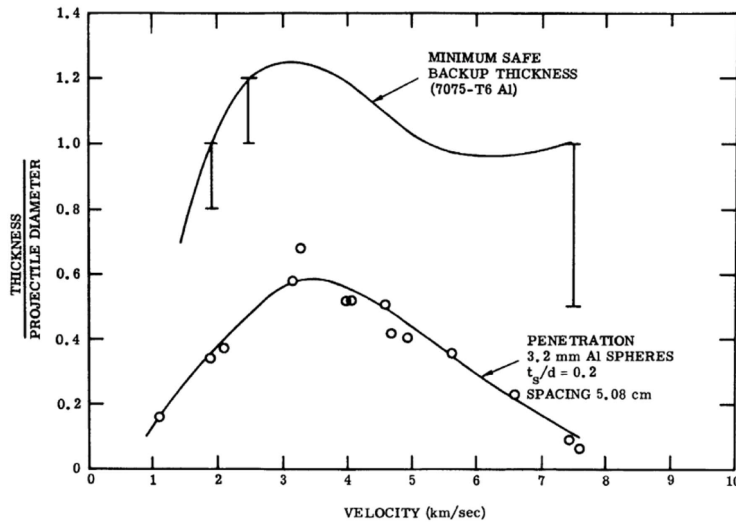


Fig. 6. Thickness of a Whipple shield rear wall required to prevent perforation (from [5]).

which is calculated from for aluminium 7075-T6 ($HB = 150$; $\rho = 2.81 \text{ g/cm}^3$, $C = 5.051 \text{ km/s}$) and a perforation failure mode (i.e., $k = 1.8$), i.e.:

$$1.8 \times 5.24 \times \frac{H^{-.25}}{\rho^{0.5} C^{2/3}} \approx 0.6 \quad (7)$$

The modified sizing equation, to prevent perforation in the low velocity regime, is thus simplified to:

$$t_w = 0.6 d_p^{19/18} \rho_p^{1/2} (\cos\theta)^{5/3} V^{2/3} \quad (8)$$

To define Whipple shield performance in the low velocity regime Eq. (8) can be rearranged to solve for d_p . In addition, a material-strength scaling term, like that in Eq. (3), is used to relate the performance to the reference aluminium alloy (AA6061-T6). Finally, the bumper thickness, t_b , is added to the rear wall thickness to represent a single sheet. The resulting NNO BLE in the low velocity regime, i.e., $V_n \leq 3 \text{ km/s}$, from [20] is given as:

$$d_c = \left[\frac{(t_w(\sigma/40)^{0.5} + t_b)}{0.6(\cos\theta)^{5/3} \rho_p^{0.5} V^{2/3}} \right]^{18/19} \quad (9)$$

For intermediate impact velocities between the low and hypervelocity regimes, partial to complete fragmentation of the projectile occurs. With increasing fragmentation, the projectile becomes less damaging to the rear wall, thus the critical projectile size increases with increasing velocity. A linear interpolation between the critical diameter at the onset of projectile fragmentation and that at which complete fragmentation of the projectile occurs, is made in the intermediate regime, i.e.

$$d_c = d_c(V_{LV}) + \frac{d_c(V_{HV}) - d_c(V_{LV})}{V_{HV} - V_{LV}} \times (V_n - V_{LV}) \quad (10)$$

where $V_{LV} = 3 \text{ km/s}$ and $V_{HV} = 7 \text{ km/s}$ for aluminium-on-aluminium impacts.

Finally, for oblique impact, Christiansen [19] found that at angles above 65° most rear wall damage is caused by bumper fragments. As such, for higher angles of obliquity, the critical particle size should be constrained to that for 65° , i.e.:

$$d_c(\theta > 65^\circ) = d_c(\theta = 65^\circ) \quad (11)$$

In Fig. 7, the NNO BLE is plotted in terms of shield performance, Eqs.

(5), (9), and (10), together with Cour-Palais' non-optimum equation (valid for application in the hypervelocity regime), Eq. (2) (rearranged to solve for d_p), and Cour-Palais' single plate equation (valid for application in the low velocity regime), Eq. (6).

5. Christiansen-modified NNO ballistic limit equation

With NASA's transition to the International Space Station (ISS) program, additional hypervelocity impact testing was conducted which broadened the impact conditions and target designs previously explored. Assessed against this enhanced database, the NNO was found to be potentially non-conservative in the hypervelocity regime for:

- Shield spacing to projectile diameter ratios (S/d_p) less than 15, and
- $(t_b \rho_b)/(d_p \rho_p)$ less than 0.18.

as initially cautioned in [21].

In [8] Christiansen and Kerr proposed several updates to the NNO equation in the low- and hyper-velocity regimes to extend the applicability of the NNO to a wider range of target conditions, including thinner bumper plates and Whipple shields that incorporated multi-layer insulation (MLI) blankets.

For Whipple shields with under-sized bumpers, the following modifications were proposed to the performance form of the BLE in the hypervelocity regime:

- Dependence of the scaling parameter, C (now k_h), on shield geometry (i.e., t_b , t_w , S),
- Extension of rear wall material property dependence to include both yield strength and density,
- Increased standoff dependence.

In the hypervelocity regime the modified NNO BLE, in performance form, is given as:

$$d_c = k_h \frac{(t_w \rho_w)^{2/3} S^{1/2}}{(V \cos\theta)^{2/3} \rho_p^{1/3} \rho_b^{1/9}} \left(\frac{\sigma_y}{70} \right)^{1/3} \quad (12)$$

$$\text{where } k_h = \begin{cases} 1.35 & \text{for } t_b/(t_w^{2/3} S^{1/3}) < 0.126 \\ 7.451 t_b/(t_w^{2/3} S^{1/3}) + 0.411 & \text{for } t_b/(t_w^{2/3} S^{1/3}) \geq 0.126 \end{cases} \quad (13)$$

The hypervelocity scaling coefficient k_h is dependent on a non-dimensional geometry coefficient, $t_b/(t_w^{2/3} S^{1/3})$. In Fig. 8 this

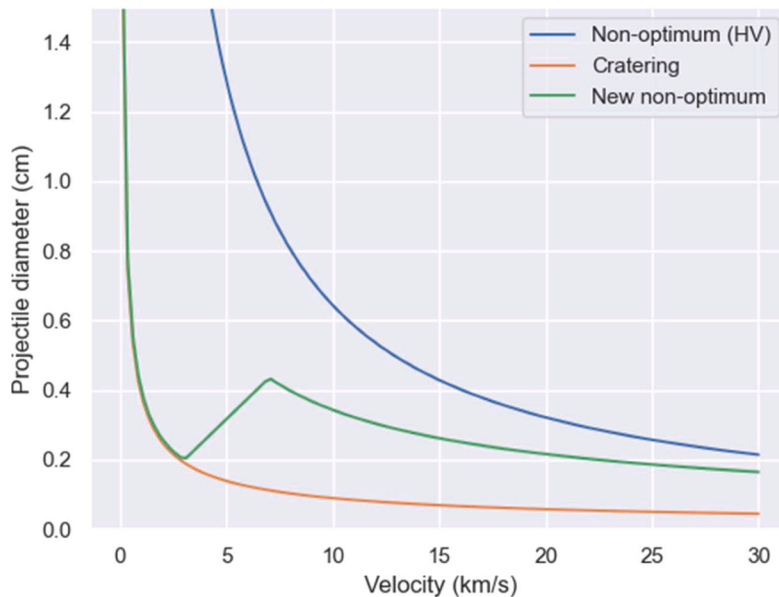


Fig. 7. Comparing the NNO ballistic limit curve for a Whipple shield with $t_b = 0.08$ cm, $t_w = 0.30$ cm, $S = 5.08$ cm, $\rho_b = 2.7$ g/cm³, $\rho_w = 2.7$ g/cm³, $\rho_p = 2.7$ g/cm³, $\sigma_w = 40$ ksi, HB_w = 95 BHN, C_w = 5.05 km/s, at normal incidence with the original non-optimum and single sheet equations from Cour-Palais.

coefficient, i.e., Eq. (13), is plotted together with experimental data from [2] that is expected to be identical (or close-to-identical) as that used to derive the modified BLE in [8]. Ideally, the fit line should separate the perforated test results (above) from the non-perforated results (below). Conservative estimations of the parameter k_h indicate those in which the non-perforated test results (black circles) are shown above the fit curve, while non-conservative estimations show perforated test results (white circles) below the fit curve.

Christiansen and Kerr also made modifications to the NNO low velocity regime, namely:

- Inclusion of bumper material properties (density), normalised to that of AA6061-T651 (i.e., $\rho_b/2.70$),
- Decrease in the cratering dependence on projectile diameter from 1.06 to 1.0,
- Increased angle dependence.

Additionally, the onset of projectile fragmentation, i.e., transition from low- to intermediate-velocity regimes, was also modified to incorporate increased angle dependence, $V_{LV} = V \cos^{1.5}\theta$.

In the low velocity regime, $V_n \leq V_{LV}$, the modified NNO BLE, in performance form, is:

$$d_c = k_l \frac{\left(t_w (\sigma/40)^{0.5} + t_b (\rho_b/2.71) \right)}{(\cos\theta)^{11/6} \rho_p^{0.5} V^{2/3}} \quad (14)$$

where $k_l = 1.9 \text{ g}^{0.5} \text{ km}^{2/3} \text{ cm}^{-3/2} \text{ s}^{-2/3}$

The modified NNO was evaluated in [8] against a database of “about 200 tests”, including:

- Projectile diameters between 0.20 and 1.9 cm
- Impact velocities from 2 to over 8 km/s
- Impact angles from 0° to 75°

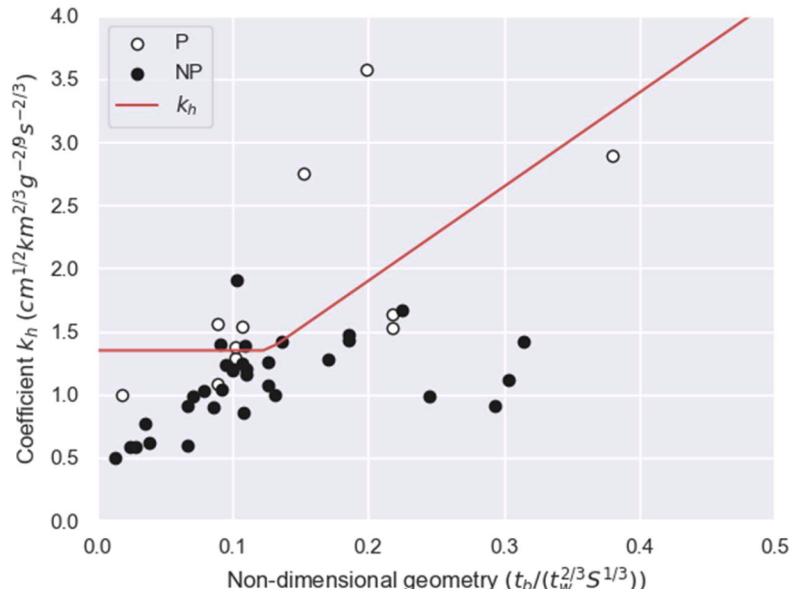


Fig. 8. Hypervelocity fit parameter, k_h , for the modified NNO BLE from [8] compared with experimental data in the hypervelocity regime from [2].

- Aluminium, copper, steel, and nylon projectiles
- t_b/d_p ratios between 0.05 to over 1.0
- S/d_p ratios between 3 to over 140

For their database the modified NNO accurately predicted over 90 % of the perforated results, compared with 77 % from the original NNO.

Unfortunately, the database used in [8] was not published. However, shortly afterwards Christiansen published [2] which contained a database of 187 impact tests on Whipple shields without MLI (once duplicates are removed). The characteristics of that database, for comparison with the characteristics of the database used in [8] listed above, are:

- Projectile diameters between 0.18 and 1.908 cm (comparable)
- Impact velocities from 2.5 to 8.06 km/s (comparable)
- Impact angles from 0° to 75° (comparable)
- Aluminium, copper, glass, and nylon projectiles (new glass entries, no steel entries)
- t_b/d_p ratios between 0.04 and 3.5 (larger upper limit)
- S/d_p ratios between 3.48 and 141 (comparable)

Using the database provided in [2] we can evaluate the performance difference between the NNO and modified NNO on a similar sized database to that used in [8], see Fig. 9. There are 61 perforation results in the database, of which the NNO correctly predicts 61 % and the modified NNO correctly predicts 56 %, i.e., well below the performance reported in [8], see Table 3.

In Fig. 10 the modified NNO ballistic limit curve is compared to that of the NNO for several target configurations repeated in the database from [2]. For most configurations the two BLEs give similar predictions although substantial deviation in the hypervelocity regime is observed for configurations based on test ID A1466 (0.2 mm AA6061-T6 bumper/19.8 mm standoff/0.2 mm AA6061-T6 rear wall, impacted at 45°).

6. Reimerdes-modified NNO ballistic limit equation

Reimerdes et al. proposed modifications to the NNO in [9] to include the effect of bumper thickness in the rear wall sizing and, subsequently, performance equations. Such modifications were required to perform numerical optimisation of Whipple shield designs, see e.g., [28].

In the low velocity regime Reimerdes, et al. [9] proposed incorporating the Fish-Summers perforation equation [29] in the form provided in [30],

$$t_w = kP_{\infty 2} = k(P_{\infty 1} - t_b) \quad (15)$$

and

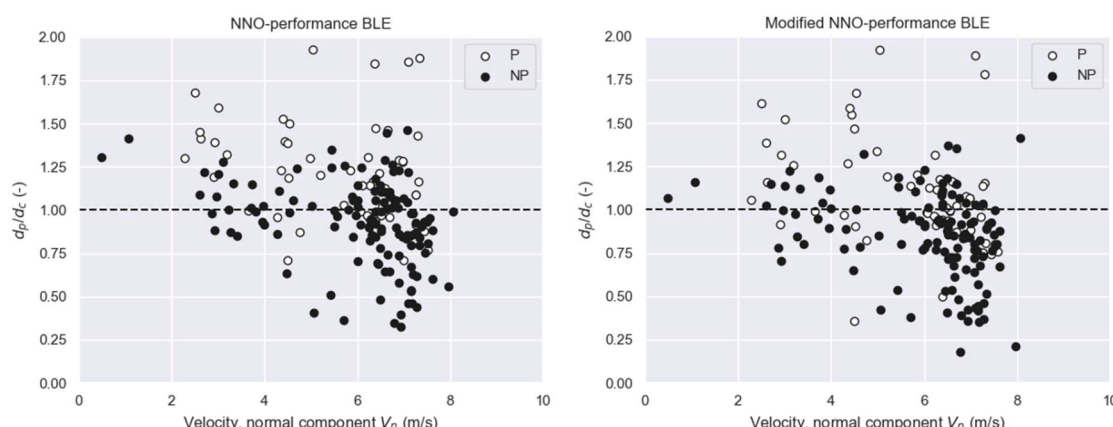


Fig. 9. Comparing the performance of the NNO (left) and modified NNO (right) for the database of 187 experiments provided in [2].

Table 3

Performance of the Christiansen and Kerr modified NNO performance BLE, Eqs. (12)-(14), applied to the database in [2] compared with that of the NNO performance BLE, Eqs. (5) & (9).

Model	Accuracy			Precision	Recall	F1-score
	Overall	“P” class	“NP” class			
NNO	0.672 (125/187)	0.607 (37/61)	0.704 (88/126)	0.500	0.607	0.548
Mod- NNO	0.672 (125/187)	0.557 (34/61)	0.728 (91/126)	0.500	0.557	0.527

$$P_{\infty 1} = K_{\infty} m_p^{0.352} \rho_p^{1/6} V_n^{2/3} \quad (16)$$

where k is a failure-mode dependent constant equal to 1.8, 2.2, or 3.0 to prevent perforation, detached spallation, or incipient spallation and K_{∞} is a material-specific constant equal to 0.42 for aluminium target plates [30].

Eq. (15), in addition to using a different form of single plate penetration equation than the NNO, explicitly reduces the required rear wall thickness in the low velocity regime by the thickness of the bumper plate.

Multiple single wall penetration equations, including the Fish-Summers and Cour-Palais expressions, were evaluated in [30] for several projectile and target configurations. In Fig. 11 we compare the single plate form of Eq. (15), i.e., $t_b = 0$, to the equations from [30].

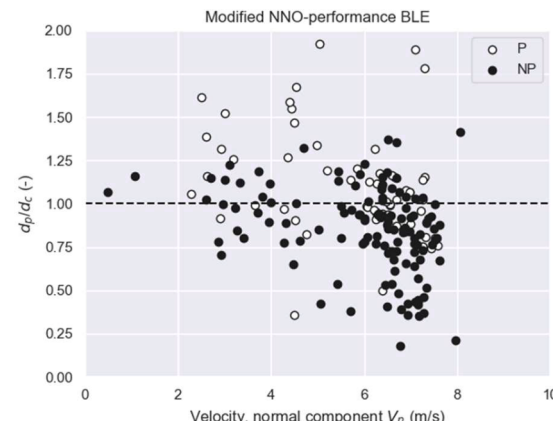
Expressed in terms of shield performance, the Reimerdes BLE in the low velocity regime, $V \leq V_{LV}$, is given by:

$$d_c = \left[\frac{t_w/k + t_b}{0.796 K_{\infty} \rho_p^{0.518} V_n^{2/3}} \right]^{18/19} \quad (17)$$

Reimerdes et al. [9] proposed a modification to the low-to-intermediate regime transition velocity, V_{LV} , based on original work by McMillan et al. [23] who found that the velocity required to induce projectile fragmentation varied with bumper thickness-to-projectile diameter ratio, t_b/d_p . Piekutowski et al. [31] confirmed McMillan's findings, the results of which are repeated in Fig. 12. For comparison, the non-optimum, new non-optimum, and Christiansen-modified new non-optimum equations all assume that the onset of projectile fragmentation is independent of bumper thickness. Reimerdes defined V_{LV} based on a regression fit to data in [31] as follows:

$$V_{LV} = 1.853 + 0.397 \left(\frac{t_b}{d_p} \right)^{-0.565} \quad (18)$$

Reimerdes et al. [9], like Christiansen and Kerr in [8], proposed



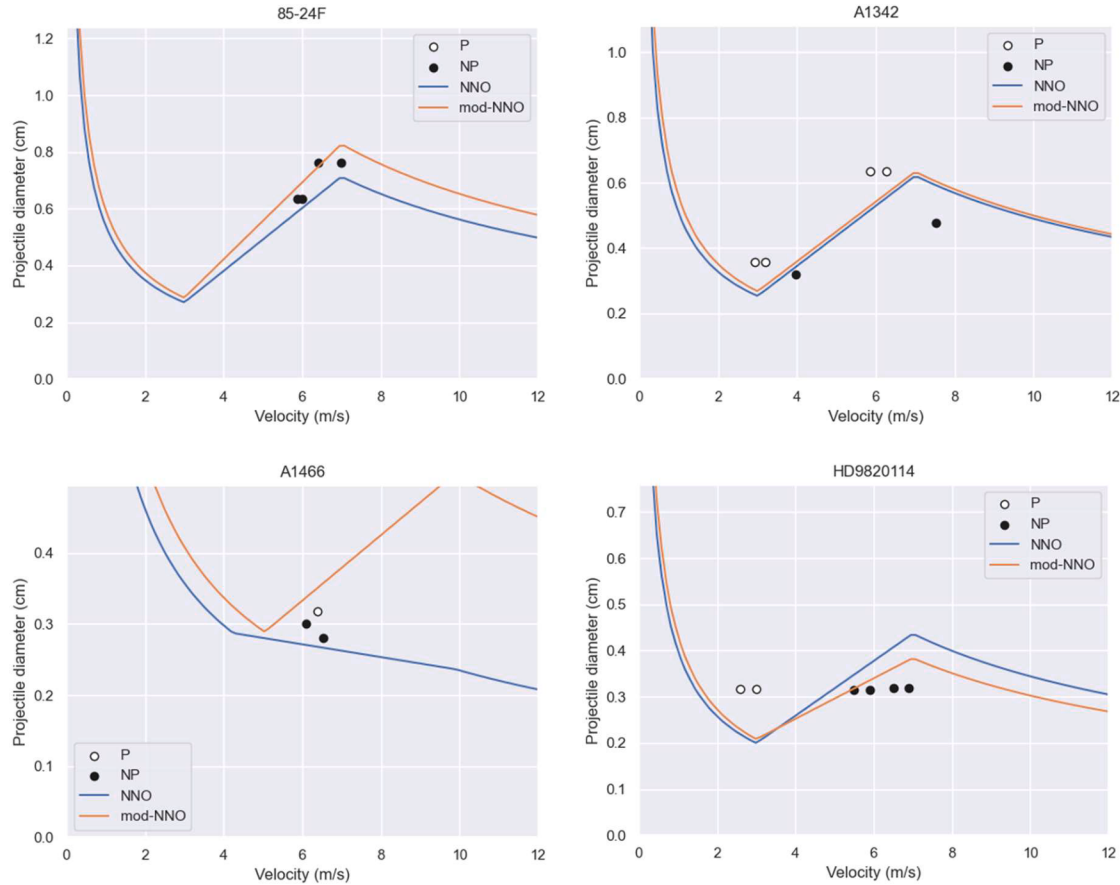


Fig. 10. Comparing the ballistic limit curves calculated by the NNO (blue line) and modified NNO (orange line) with experimental data from [2]. Plot titles refer to test IDs from [2] that define the Whipple shield configuration.

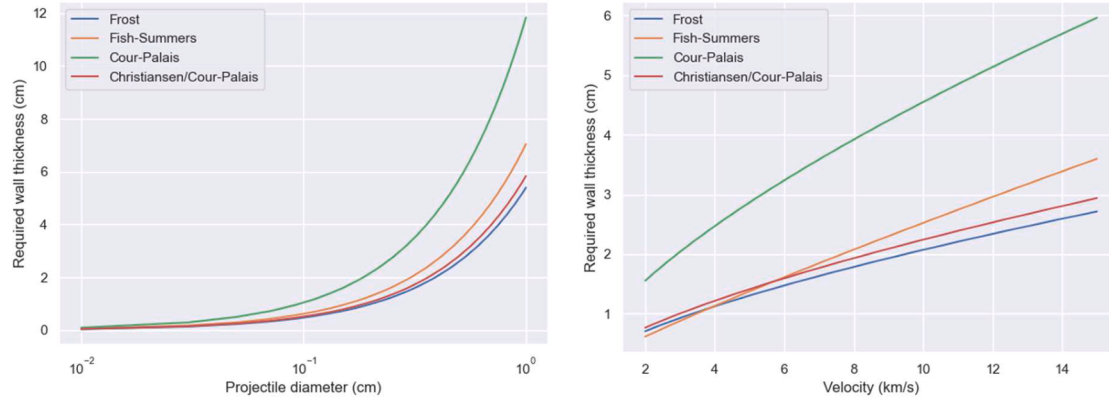


Fig. 11. Comparison of single-wall penetration equations in terms of projectile diameter (left) at a fixed velocity of 14 km/s and impact velocity (right) for a fixed projectile diameter of 0.5 cm.

modifications to the NNO to account for very thin bumper plates in the hypervelocity regime. Reimerdes proposed a de-rating factor, F_2^* , which is aimed at reproducing the rapid increase in required rear wall thickness for Whipple shields with insufficiently thick bumper plates to effectively fragment the impacting projectile (after [23]).

The Reimerdes modification in the hypervelocity regime is given as:

$$t_w = 0.178 F_2^{* -1/2} \frac{m_p^{1/2} \rho_b^{1/6}}{S^{1/2}} V_n \left(\frac{70}{\sigma_y} \right)^{1/2} \quad (19)$$

for design calculations, and:

$$d_c = 3.918 F_2^{*-2/3} \frac{t_w^{2/3} S^{1/3}}{(V \cos \theta)^{2/3} \rho_p^{1/3} \rho_b^{1/9}} \left(\frac{\sigma_y}{70} \right)^{1/3} \quad (20)$$

for performance calculations, where $F_2^* = 1$ for a ‘correctly’ sized bumper (after Christiansen [4]), and $F_2^* < 1$ for insufficiently sized bumper plates, based on a quadratic fit anchored by the following points:

1. At $t_b/d_p = (t_b/d_p)_{crit}$, as defined by Eq. (4), the rear wall thickness is the same as that calculated by the NNO.

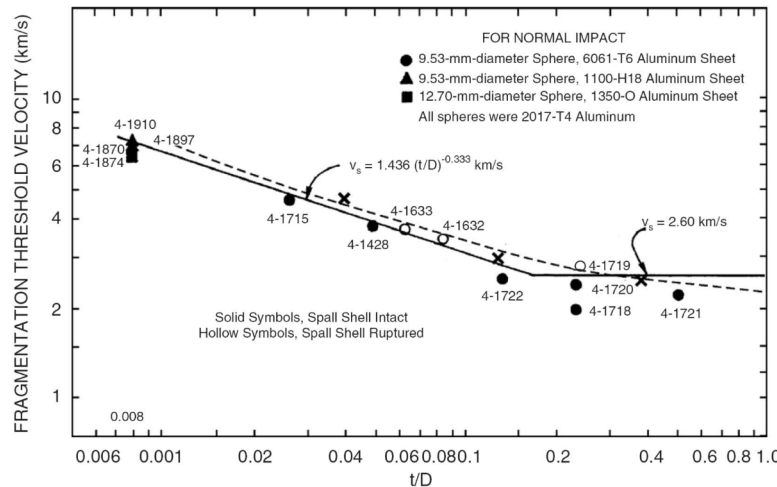


Fig. 12. The onset of projectile fragmentation for spherical aluminium-on-aluminium impacts in terms of bumper thickness, t , to projectile diameter, D , from [31]. Reimerdes et al. [9] fit a regression to Piekutowski's data, shown by the dashed line, which is used to calculate V_{LV} .

2. At $t_b = 0$, the critical projectile diameter is the same as that calculated using a single wall penetration equation, i.e., Eq. (17).
3. The slope of the de-rated performance, defined by F_2^* , should converge steadily with the NNO, i.e., $dF_2^*/d(t_b/d_p) = 0.0$ at $(t_b/d_p)_{crit}$.

and

$$(t_b/d_p)_{crit} = \begin{cases} 0.25 & \text{for } S/d_p < 30 \\ 0.20 & \text{for } S/d_p \geq 30 \end{cases} \quad (23)$$

$$F_2^* = \begin{cases} 1 & \text{for } (t_b/d_p) \geq (t_b/d_p)_{crit} \\ r_{S/D} - 2 \frac{(t_b/d_p)}{(t_b/d_p)_{crit}} (r_{S/D} - 1) + \left(\frac{(t_b/d_p)}{(t_b/d_p)_{crit}} \right)^2 (r_{S/D} - 1) & \text{for } (t_b/d_p) < (t_b/d_p)_{crit} \end{cases} \quad (21)$$

$$r_{S/D} = \frac{t_w(t_b = 0)}{t_w(t_b/d_p = (t_b/d_p)_{crit})} \text{ at } 7 \text{ km/s} \quad (22)$$

after Eq. (4)

The value of F_2^* , with respect to t_b/d_p , is plotted in Fig. 13 for two differently spaced Whipple shields.

The coefficient $r_{S/D}$ is the ratio of the required thickness of a rear wall when the thickness of the bumper plate is zero, $t_w(t_b = 0)$, i.e., the single

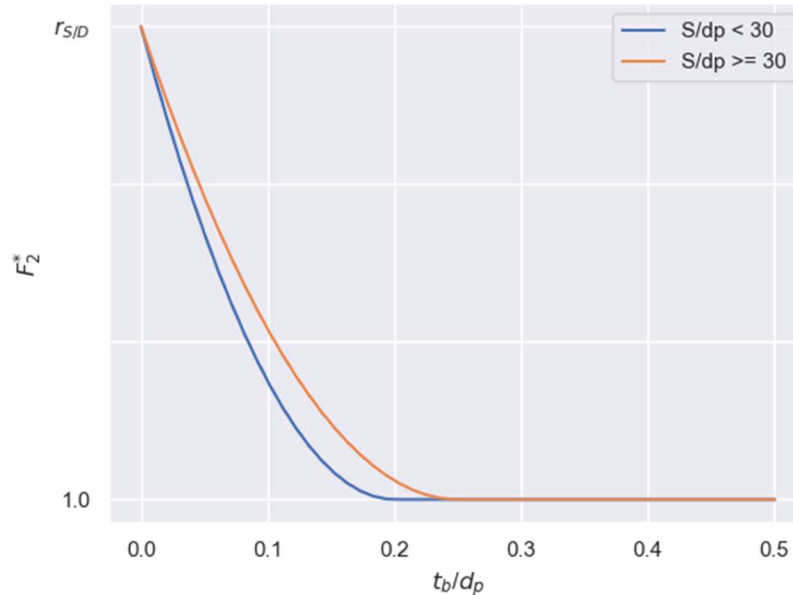


Fig. 13. Reimerdes de-rating factor F_2^* applied to Whipple shield configurations with insufficiently thick bumper plates in the hypervelocity regime.

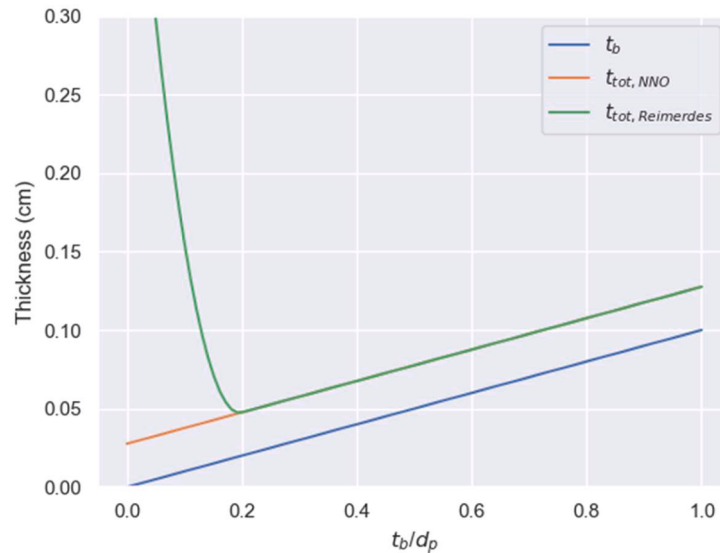


Fig. 14. Required total Whipple shield thickness ($t_b + t_w$) in terms of bumper thickness to projectile diameter ratio, showing the effect of the Reimerdes F_2^* de-rating factor in the hypervelocity regime for under-sized bumper plates.

plate penetration equation, to the thickness of a rear wall when the bumper thickness is equal to the critical thickness defined by Eq. (23), $t_w(t_b/d_p = (t_b/d_p)_{\text{crit}})$ at 7 km/s impact velocity, i.e.:

$$r_{S/D} = \frac{1.8 \left(0.42 m_p^{0.352} \rho_p^{1/6} (V_{HV} \cos \theta)^{2/3} - 0 \right)}{0.178 m_p^{1/2} \rho_p^{1/6} (V_{HV} \cos \theta) S^{-1/2} (70/\sigma_y)^{1/2}} \quad (24)$$

The effect of the F_2^* de-rating factor is plotted in Fig. 14 for a generic Whipple shield design. Here we can observe that the de-rating factor results in a rapid increase in required rear wall thickness as the bumper plate thickness reduces below the critical threshold, Eq. (23). The effect of the de-rating factor is shown to agree very well with the experimental observations in, e.g., [23].

Solving the Reimerdes-modified NNO BLE in the performance form, i.e., Eq. (20), is more complicated than the original NNO or Christiansen-modified NNO as the de-rating factor, F_2^* , is recursive with projectile diameter. Thus, Eqs. (20) and (21) must either be solved iteratively or simultaneously. Additionally, the surface described by the F_2^* is

discontinuous in t_b/d_p due to Eq. (23), shown in Fig. 15. As a result, gradient descent-based numerical solvers can have difficulty with calculating F_2^* for some target geometries.

The Reimerdes modifications are depicted in Fig. 16, compared with the original NNO BLE. As the bumper thickness decreases beyond the critical limit defined by Eq. (23), the Reimerdes modification predicts substantially degraded shielding performance in the hypervelocity regime.

The Reimerdes modifications to the NNO were verified on a series of 8 tests in [9], primarily for the hypervelocity regime modifications. No experimental justification for the low velocity regime modifications is provided.

7. JSC Whipple shield ballistic limit equation

Ryan and Christiansen incorporated several, but not all of Reimerdes' modifications in the JSC Whipple BLE [10]. In the low velocity regime, the original form of the NNO was retained, primarily due to the

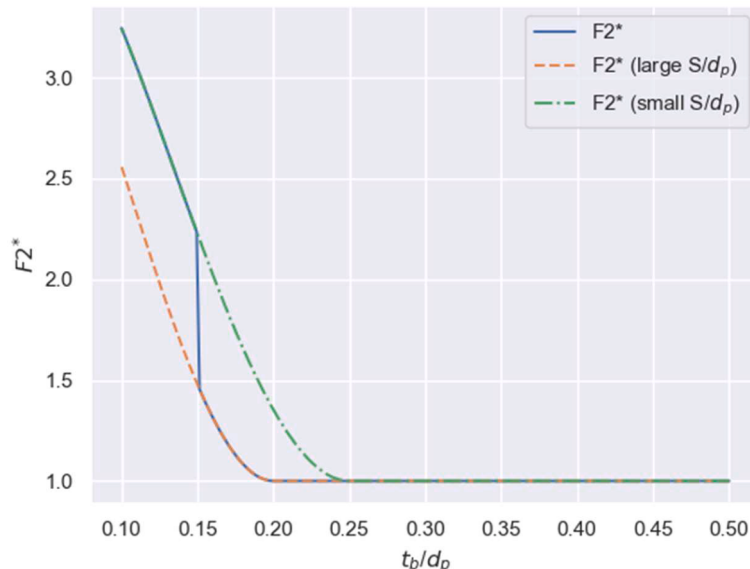


Fig. 15. Discontinuity of the Reimerdes F_2^* de-rating factor in terms of t_b/d_p due to Eq. (23).

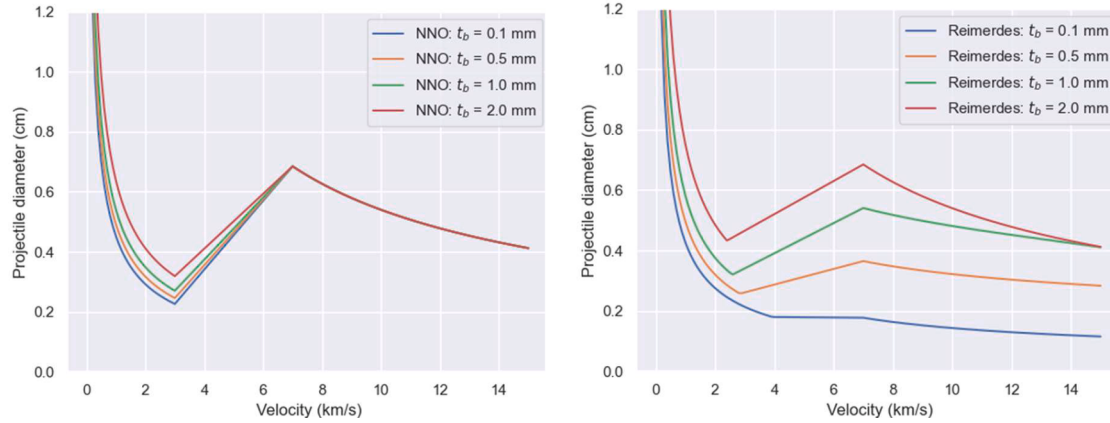


Fig. 16. Comparing the NNO (left) and Reimerdes (right) ballistic limit curves for a Whipple shield with $S = 10.0$ cm, $t_w = 0.4$ cm, $\rho_p = 2.8$ g/cm 3 , $\rho_b = 2.77$ g/cm 3 , $\sigma_w = 45$ ksi, and varying bumper thickness at normal incidence.

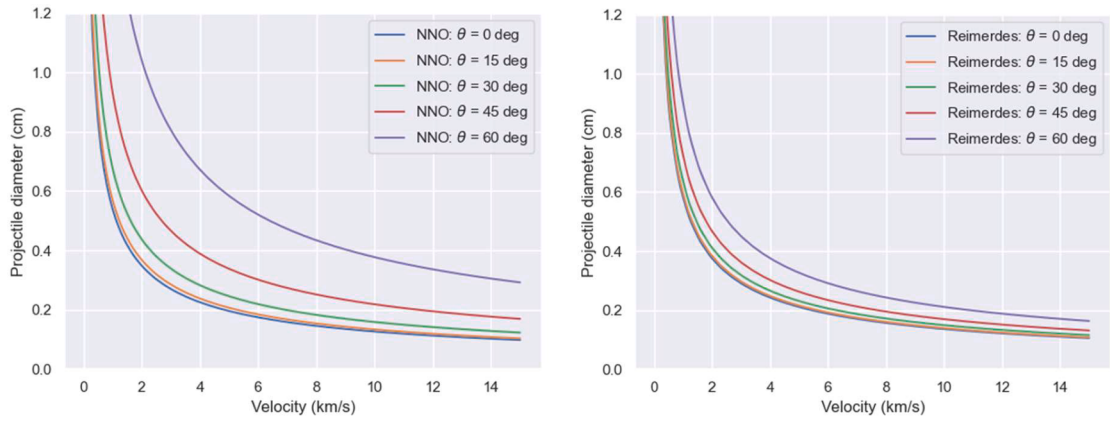


Fig. 17. Comparing the angle dependency of the NNO/JSC Whipple (left) and Reimerdes (right) ballistic limit curves in the low velocity regime for a Whipple shield with $S = 10.0$ cm, $t_b = 0.1$ cm, $t_w = 0.4$ cm, $\rho_p = 2.8$ g/cm 3 , $\rho_b = 2.77$ g/cm 3 , $\sigma_w = 45$ ksi, and varying impact obliquity. The curves are plotted for velocities beyond the low velocity transition limit for illustration.

increase in angle dependency introduced by Christiansen for the inclusion of slant range (see section 4). In terms of the performance equation, the low velocity form of the NNO and Reimerdes BLEs are compared below and are plotted in Fig. 17 for a representative Whipple shield.

Reimerdes (based on Fish – Summers) :

$$d_c = \left[\frac{t_w/1.8 + t_b}{0.334 \rho_p^{0.518} (\cos\theta)^{2/3} V^{2/3}} \right]^{18/19} \quad (25)$$

NNO/JSC Whipple (based on Cour – Palais) :

$$d_c = \left[\frac{t_w(\sigma/40)^{0.5} + t_b}{0.6 \rho_p^{0.5} (\cos\theta)^{5/3} V^{2/3}} \right]^{18/19} \quad (26)$$

It is apparent that the Whipple shield performance in the low velocity regime is predicted to increase more substantially with impact obliquity by the NNO/JSC Whipple than by the Reimerdes BLE.

The JSC Whipple BLE incorporated Reimerdes' F_2^* de-rating factor, Eq. (21), in the hypervelocity regime without change. However, the different low velocity form of the JSC Whipple BLE affects the F_2^* de-rating factor through the $r_{S/D}$ term. For the JSC Whipple BLE the rS/D is explicitly calculated as:

$$\begin{aligned} r_{S/D} &= \frac{t_w(t_b = 0)}{t_w \left(t_b / d_p = (t_b / d_p)_{crit} \right)} \\ r_{S/D} &= \frac{0.6 d_p^{19/18} \rho_p^{0.5} (\cos\theta)^{5/3} V_{HV}^{2/3} (40/\sigma_y)^{1/2}}{0.16 d_p^{1/2} (\rho_p \rho_b)^{1/6} m_p^{1/3} (V_{HV} \cos\theta) S^{-1/2} (70/\sigma_y)^{1/2}} \end{aligned} \quad (27)$$

compared to Eq. (24) for the Reimerdes BLE, repeated here:

$$r_{S/D} = \frac{1.8 \left(0.42 m_p^{0.352} \rho_p^{1/6} (V_{HV} \cos\theta)^{2/3} - 0 \right)}{0.178 m_p^{1/2} \rho_b^{1/6} (V_{HV} \cos\theta) S^{-1/2} (70/\sigma_y)^{1/2}}$$

The JSC Whipple BLE also adopted a bumper-thickness dependent velocity for the onset of projectile fragmentation (i.e., V_{LV}), as proposed by Reimerdes in [9]. However, the original form proposed by Piektowski et al. in [31] and shown in Fig. 12 was used, rather than the modification proposed by Reimerdes et al., Eq. (18). The V_{LV} transition velocity for the JSC Whipple BLE is given as:

$$V_{LV} = \begin{cases} 1.436 (t_b/d_p)^{-1/3} & \text{for } t_b/d_p < 0.16 \\ 2.60 & \text{for } t_b/d_p \geq 0.16 \end{cases} \quad (28)$$

Evaluation of the JSC Whipple BLE was performed with a database of 444 impact tests from a range of sources, including [2,4,5,9,32]. We evaluated the NNO, Christiansen and Kerr modified-NNO, Reimerdes modified-NNO, and JSC Whipple against this database and provide the results in Fig. 18 and Table 4. From the table we can observe that the

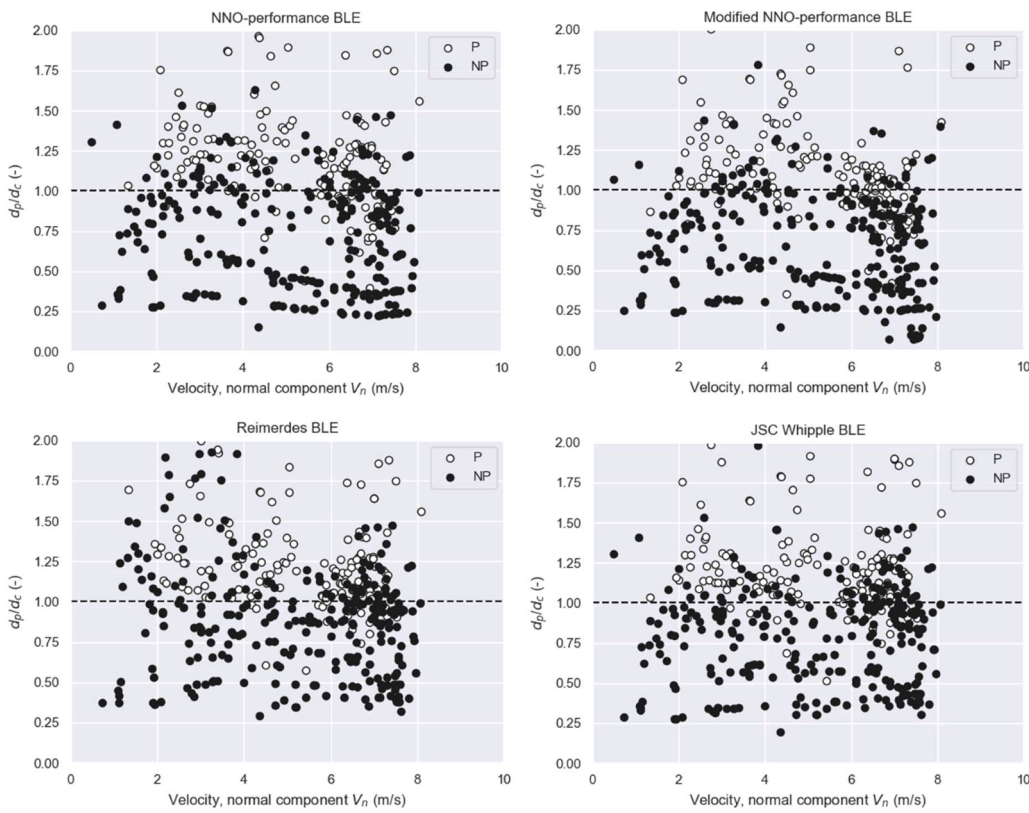


Fig. 18. Comparing the performance of the NNO (top left), Christiansen and Kerr modified NNO (top right), Reimerdes et al. modified NNO (bottom left) and JSC Whipple BLEs (bottom right) for the database of 444 experiments used in [10].

Table 4

Comparing the performance of different performance BLEs applied to a database of 444 impact experiments from a range of sources, originally used in the evaluation of the JSC Whipple BLE [10]. Best scoring model(s) for each metric are indicated in bold.

Model	Accuracy			Precision	Recall	F1-score
	Overall	“P” class	“NP” class			
NNO	0.761 (338/444)	0.766 (121/158)	0.759 (217/286)	0.637	0.766	0.695
Mod-NNO	0.784 (348/444)	0.658 (104/158)	0.853 (244/286)	0.712	0.658	0.684
Reimerdes	0.721 (320/444)	0.842 (133/158)	0.654 (187/286)	0.573	0.842	0.682
JSC Whipple	0.784 (348/444)	0.861 (136/158)	0.739 (212/286)	0.648	0.861	0.739

Christiansen and Kerr modified-NNO and the JSC Whipple have the best classification accuracy of the four methods evaluated. However, the Christiansen and Kerr modified NNO has the most non-conservative predictions (false negatives) of all four models, realisable in the poor recall score. The Reimerdes modified NNO shows significantly improved recall over the original NNO (i.e., reduced number of non-conservative predictions), albeit at the cost of reduced precision (i.e., reduced accuracy in predicting NP results). The JSC Whipple equation, in comparison with the Reimerdes modification, retains the improved ability to predict perforation results, resulting in a comparable recall score, without any loss in precision compared to the NNO. This is primarily due to the conservative behaviour of the Reimerdes equation in the low velocity regime, particularly for oblique impacts. In Fig. 18a comparison between the Reimerdes and JSC Whipple plots shows a greater population of NP points above $d_p/d_c = 1$ in the low velocity regime – this is a visualisation of that LV regime conservatism.

Ballistic limit curves are plotted in Fig. 19 for a selection of Whipple shields from the database of 444 impact tests discussed above. For

Whipple shields with ‘sufficiently’ thick bumper plates, e.g., those used in A1342, etc., the variation between models is minimal. For oblique impacts, e.g., A1487, etc., or those with very thin bumper plates, e.g., 1794, etc., the variation is substantial. For configuration A1672 we can observe that the Reimerdes and JSC Whipple curves are relatively flat between approx. 7–8.5 km/s. At these velocities both the (t_b/d_p) and (S/d_p) ratios are transitioning across the limits defined in Eqs. (21)–(23), such that the value of F_2^* is increasing from an initial value <1 to 1, eventually collapsing upon the NNO curve.

7.1. A note on the application of the JSC Whipple BLE

The added complexity of the Reimerdes and JSC Whipple BLE over the conventional NNO related to calculation of the F_2^* de-rating factor introduces some challenges. There have also been several errors in the reporting of both equations, further complicating their correct implementation. In the original Reimerdes publication [9], the general formulation of F_2^* is incorrectly given as:

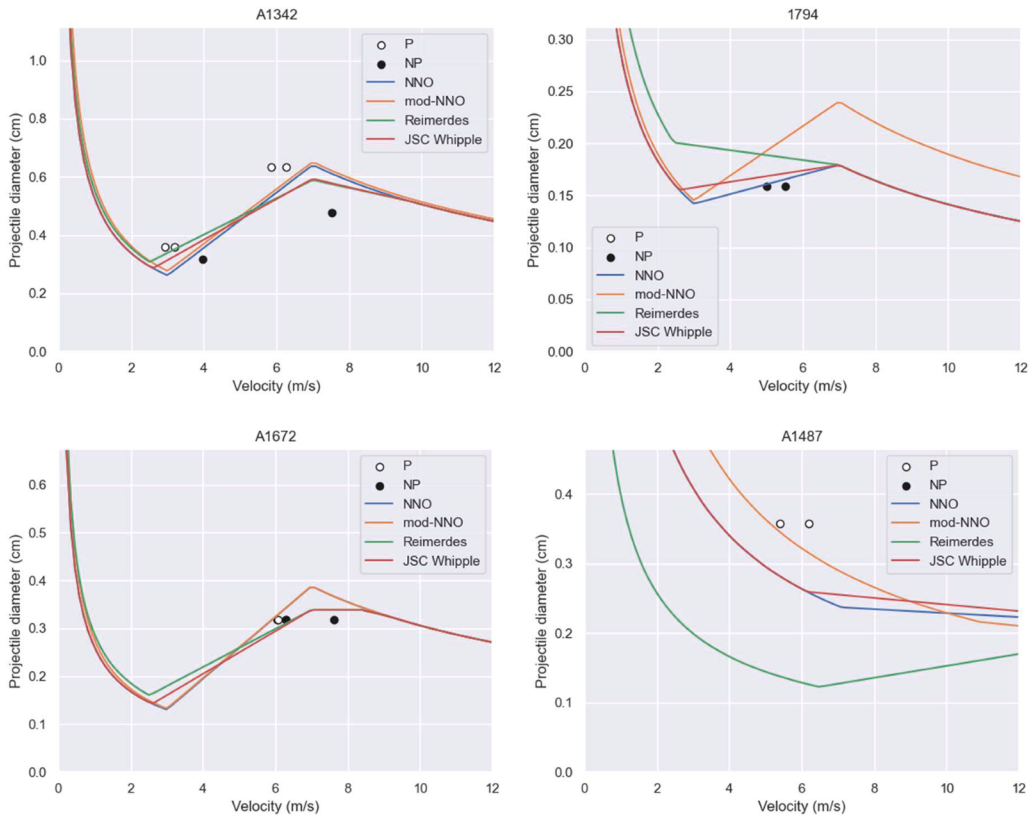


Fig. 19. Comparing ballistic limit curves generated by the NNO, Christiansen and Kerr modified NNO (mod-NNO), Reimerdes modified NNO, and JSC Whipple BLE. Plot titles refer to test IDs from [10] that define the Whipple shield configuration.

$$F_2^* = \begin{cases} 1 & \text{for } (t_b/d_p) \geq (t_b/d_p)_{crit} \\ r_{S/D} - 10 \frac{t_b}{d_p} (r_{S/D} - 1) + 25 \left(\frac{t_b}{d_p} \right)^2 (r_{S/D} - 1) & \text{for } (t_b/d_p) < (t_b/d_p)_{crit} \end{cases} \quad (29)$$

which is repeated in [22]. However, Eq. (29) is not the general formulation of F_2^* . In their accompanying conference presentation, [33], Reimerdes et al. provided the following, correct, general formulation for F_2^* :

$$F_2^* = \begin{cases} 1 & \text{for } (t_b/d_p) \geq (t_b/d_p)_{crit} \\ r_{S/D} - 2 \frac{(t_b/d_p)}{(t_b/d_p)_{crit}} (r_{S/D} - 1) + \left(\frac{(t_b/d_p)}{(t_b/d_p)_{crit}} \right)^2 (r_{S/D} - 1) & \text{for } (t_b/d_p) < (t_b/d_p)_{crit} \end{cases} \quad (30)$$

where:

$$r_{S/D} = \frac{t_w(t_b = 0)}{t_w(t_b/d_p = (t_b/d_p)_{crit})} \quad \text{at } V = 7 \text{ km/s} \quad (31)$$

and

$$(t_b/d_p)_{crit} = \begin{cases} 0.25 & \text{for } S/d_p < 30 \\ 0.20 & \text{for } S/d_p \geq 30 \end{cases} \quad (32)$$

Indeed, the form of F_2 in Eq. (29) is actually Eq. (30) for the specific condition $S/d_p \geq 30$. Similarly, for the specific condition $S/d_p < 30$ the

equation can be simplified to:

$$F_2^* = \begin{cases} 1 & \text{for } (t_b/d_p) \geq (t_b/d_p)_{crit} \\ r_{S/D} - 8 \frac{t_b}{d_p} (r_{S/D} - 1) + 16 \left(\frac{t_b}{d_p} \right)^2 (r_{S/D} - 1) & \text{for } (t_b/d_p) < (t_b/d_p)_{crit} \end{cases} \quad (33)$$

where:

$$r_{S/D} = \frac{t_w(t_b = 0)}{t_w(t_b/d_p = (t_b/d_p)_{crit})} \quad \text{at } V = 7 \text{ km/s} \quad (34)$$

and:

$$(t_b/d_p)_{crit} = \begin{cases} 0.25 & \text{for } S/d_p < 30 \\ 0.20 & \text{for } S/d_p \geq 30 \end{cases} \quad (35)$$

In [10] the correct form for F_2^* is reported, however the value of $(t_b/d_p)_{crit}$ is incorrectly provided as a constant 0.25 rather than the S/d_p dependent form from Eqs. (35) and (23). There is an additional error in

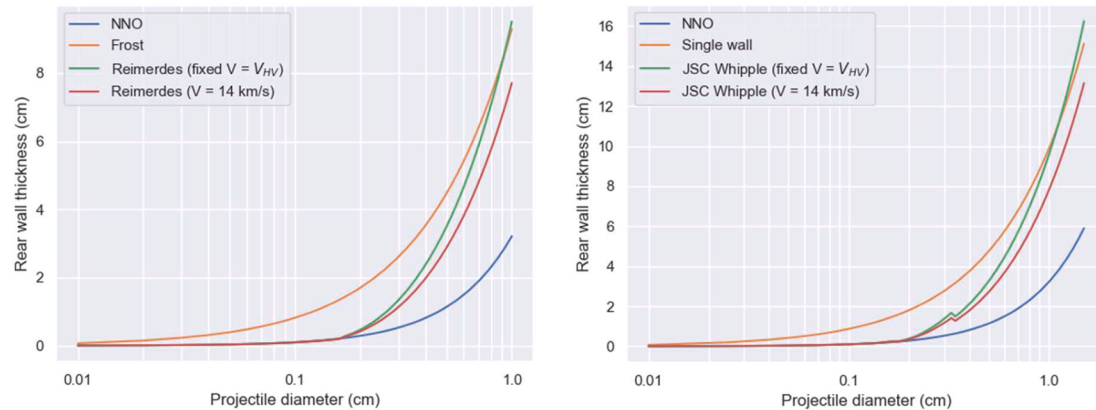


Fig. 20. Required rear wall thickness calculated with the Reimerdes BLE (left) and JSC Whipple BLE (right) for impact of a stainless-steel projectile ($\rho_p = 8.0 \text{ g/cm}^3$) at 14 km/s with normal incidence against a Whipple shield with the following parameters: $S = 5.08 \text{ cm}$, $\rho_b = 2.7 \text{ g/cm}^3$, $\sigma_y = 40 \text{ ksi}$, $t_b = 0.034 \text{ cm}$, normal impact. 'Fixed $V = V_{HV}$ ' indicates that the rear wall thickness has been calculated using $r_{S/D}$ evaluated at V_{HV} (i.e., 7 km/s), compared with ' $V = 14 \text{ km/s}$ ' where $r_{S/D}$ is evaluated at the actual impact velocity, as proposed in [34].

[10], where the negative 2/3 exponent that should be applied to the de-rating factor, F_2^* , in the performance equation is missing, as identified in [34]. It should be noted that the implementation of the Reimerdes and JSC Whipple equation in the accompanying software, [35], and the BUMPER risk assessment code correctly included the $-2/3$ exponent.

In [34] the NASA Engineering Safety Center reviewed the application of the Reimerdes F_2^* de-rating factor in the JSC Whipple equation as part of the MMOD risk assessment for the Joint Polar Satellite System (JPSS). In addition to identifying the missing $-2/3$ rd exponent on F_2^* in [10], the authors made the following suggestions:

- The $r_{S/D}$ ratio, when calculated at intermediate-to-hypervelocity regime transition, V_{HV} , equal to 7.0 km/s for normal impact of aluminium projectiles on aluminium bumpers, results in critical rear wall thicknesses that can exceed those calculated with a single wall BLE (i.e., the performance of the Whipple shield is worse than that of a similarly sized single plate). Rather, $r_{S/D}$ should be calculated at the actual normal impact velocity of the design particle.

- The recursive relationship between F_2^* and d_c in the Reimerdes modification can be replaced by a procedure by which the NNO is used to calculate required rear wall thickness for given projectile diameters and the de-rating can be applied based on an interpolation of critical diameters calculated for actual Whipple shield wall thicknesses with negligible error.

Regarding the velocity at which $r_{S/D}$ should be calculated, in Fig. 20 we reproduce a version of the plot from [34] for both the Reimerdes and JSC Whipple equations. The plot shows that if $r_{S/D}$ is calculated at $V = V_{HV}$, as directed by Reimerdes in [9], for some conditions the required rear wall thickness exceeds that of the respective single wall equations.

From section 6 we can recall that the F_2^* factor was merely a quadratic fit between the single wall equation at $t_b = 0$ and the NNO BLE at $(t_b/d_p) = (t_b/d_p)_{crit}$. At $t_b = 0$ we calculate F_2^* :

$$F_2^* = r_{S/D} - 2 \frac{(0/d_p)}{(t_b/d_p)_{crit}} (r_{S/D} - 1) + \left(\frac{(0/d_p)}{(t_b/d_p)_{crit}} \right)^2 (r_{S/D} - 1) = r_{S/D}$$

Thus, the required rear wall thickness when $t_b = 0$ is calculated as:

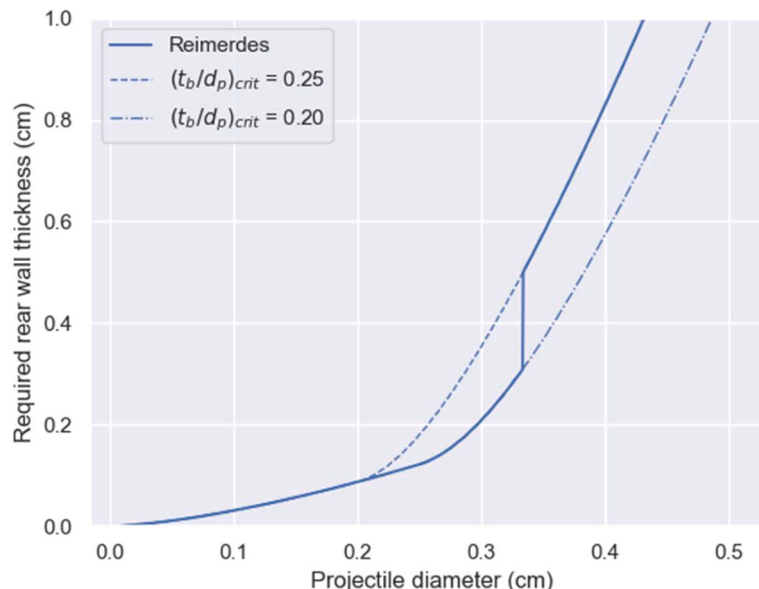


Fig. 21. Required rear wall thickness of a Whipple shield calculated using the Reimerdes sizing equation, Eq. (19), exhibiting a discontinuity at $d_p = 0.33 \text{ cm}$ related to the critical bumper sizing relationship of Christiansen. The transition of S/d_p across the threshold equal to 30 results in a discontinuous transition between conditions.

$$t_w(t_b = 0) = t_{w,NNO}(V = V) \times r_{S/D} = t_{w,NNO} \times \frac{t_w(t_b = 0)}{t_w(t_b/d_p = (t_b/d_p)_{crit})}$$

For this equation to converge with the single wall equation (given by the $r_{S/D}$ numerator), we must have:

$$t_{w,NNO} = t_w(t_b/d_p = (t_b/d_p)_{crit})$$

which is only true if $t_w(t_b/d_p = (t_b/d_p)_{crit})$ is assessed at the actual impact velocity rather than the V_{HV} transition velocity, as proposed in [34].

Regarding the recursive calculation of F_2^* and d_c , we note that the computational burden of a gradient descent-based algorithm is trivial and, as such, interpolation approaches such as that proposed in [34] should be unnecessary. However, the discontinuous nature of F_2^* , see Fig. 15, can be problematic. In section 7.2 we present a simple modification to the JSC Whipple BLE to simplify this issue.

7.2. Modifications to the JSC Whipple BLE

Consider a Whipple shield with the following characteristics: $t_b = 0.05$ cm; $S = 10.0$ cm; $\sigma_y = 70$ ksi; $\rho_b = 2.7$ g/cm³. In Fig. 21 the required rear wall thickness is calculated for impact of AA2017-T4 projectiles ($\rho_b = 2.8$ g/cm³) of varying diameter at normal incidence ($\theta = 0^\circ$). The discontinuity in the curve at $d_p = 0.33$ cm occurs when the S/d_p ratio reduces below the threshold of 30, resulting in a change of critical bumper thickness to projectile diameter ratio, $(t_b/d_p)_{crit}$, from 0.20 to 0.25. In other words, a Whipple shield designed using the Reimerdes BLE (and similarly, the JSC Whipple BLE) with the above parameters

$$F_2^* = \begin{cases} 1 & \text{for } (t_b/d_p) \geq (t_b/d_p)_{crit} \\ r_{S/D} - 2 \frac{(t_b/d_p)}{(t_b/d_p)_{crit}} (r_{S/D} - 1) + \left(\frac{(t_b/d_p)}{(t_b/d_p)_{crit}} \right)^2 (r_{S/D} - 1) & \text{for } (t_b/d_p) < (t_b/d_p)_{crit} \end{cases}$$

will need a rear wall thickness of at least 0.15 cm to defeat a projectile of diameter 0.33 cm, increasing to a required rear wall thickness of 0.26 cm to defeat a projectile diameter of 0.34 cm. This discontinuity, or ‘bump’ after [36], has no physical justification, it is merely an artifact of Christiansen’s extension of the non-optimum equation to prevent

undersized bumper plates.

A simple linear interpolation is proposed, while also retaining the bumper and projectile density dependency from the original NNO [4], i.e.:

$$(t_b/d_p)_{crit} = \begin{cases} 0.25 \rho_p / \rho_b & \text{for } S/d_p \leq 15 \\ \left(0.25 - \frac{(0.25 - 0.20)}{30 - 15} (S/d_p - 15) \right) \rho_p / \rho_b & \text{for } 15 < S/d_p < 30 \\ 0.20 \rho_p / \rho_b & \text{for } S/d_p \geq 30 \end{cases} \quad (36)$$

The effect of the modification is shown in Fig. 22. In addition to providing a smooth transition between the ‘large’ and ‘small’ S/d_p conditions the proposed modification simplifies the model for implementation in numerical solvers.

The correction to calculation of F_2^* proposed by Squire et al. in [34] is also incorporated in the hypervelocity regime, i.e.:

Design :

$$t_w = \frac{0.16 F_2^* d_p^{1/2} (\rho_p \rho_b)^{1/6} m_p^{1/3} V_n}{S^{1/2}} \left(\frac{70}{\sigma_y} \right)^{1/2} \quad (37)$$

Performance :

$$d_c = 3.918 F_2^{*-2/3} \frac{t_w^{2/3} S^{1/3}}{(V \cos \theta)^{2/3} \rho_p^{1/3} \rho_b^{1/9}} \left(\frac{\sigma_y}{70} \right)^{1/2} \quad (38)$$

where:

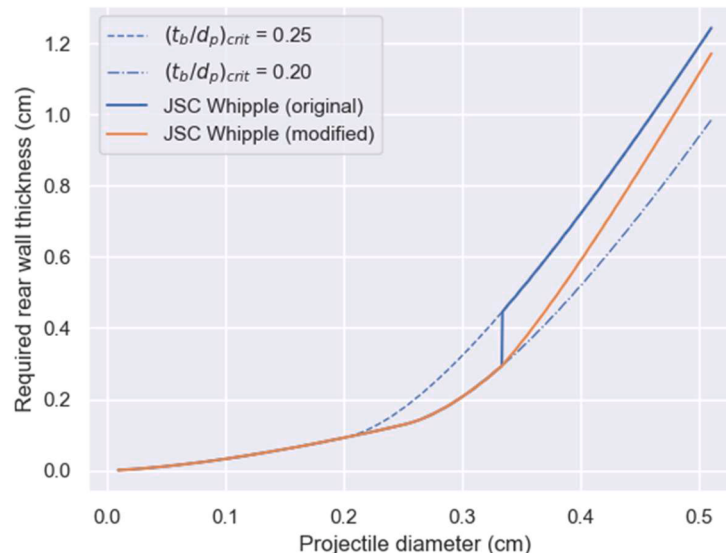


Fig. 22. A proposed modification of the critical bumper thickness to projectile diameter ratio of the F_2^* de-rating factor used in the modified JSC Whipple BLE.

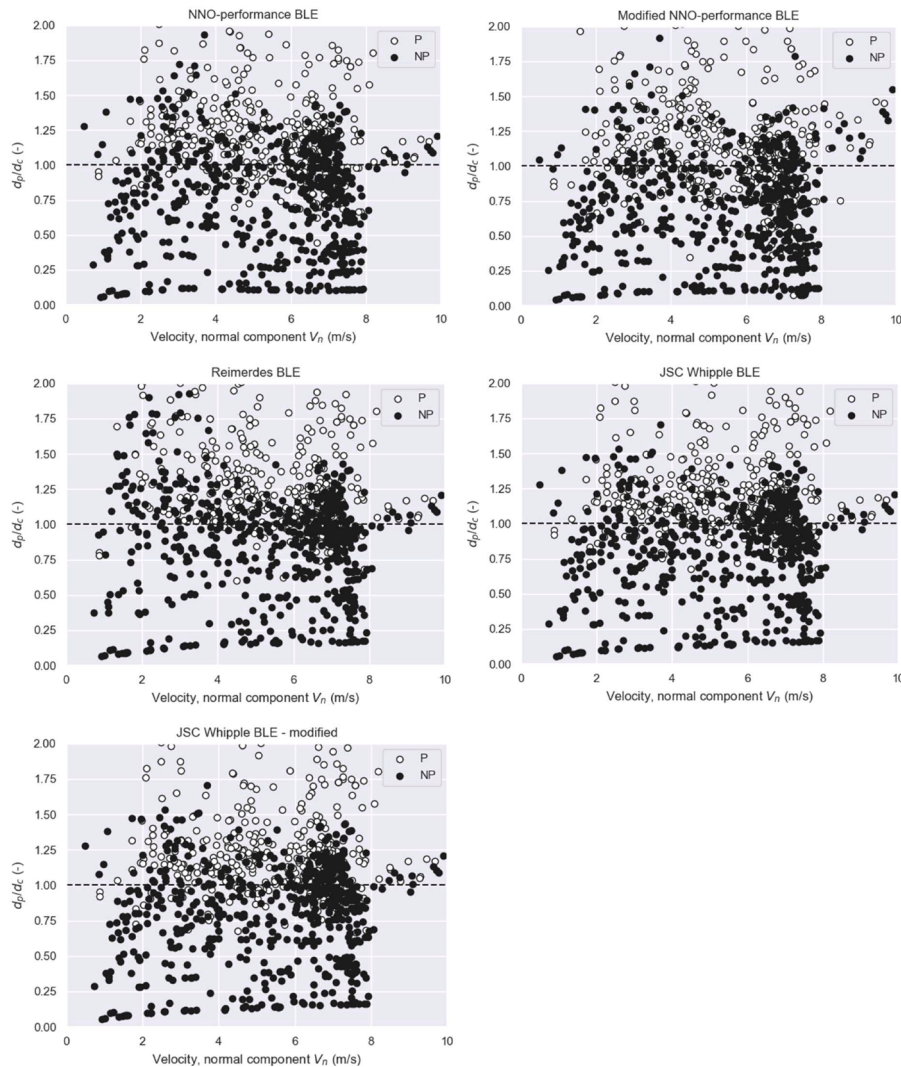


Fig. 23. Comparing the performance of the NNO (top left), Christiansen and Kerr modified NNO (top right), Reimerdes et al. modified NNO (middle left), JSC Whipple (middle right) and modified JSC Whipple (bottom left) for the database of 1135 experiments.

Table 5

Comparing the performance of different performance BLEs applied to a database of 1135 impact experiments. Best scoring model(s) for each metric are indicated in bold.

Model	Accuracy			Precision	Recall	F1-score
	Overall	“P” class	“NP” class			
NNO	0.731 (830/1135)	0.759 (399/526)	0.708 (431/609)	0.692	0.759	0.723
Mod-NNO	0.730 (828/1135)	0.673 (354/526)	0.778 (474/609)	0.724	0.673	0.698
Reimerdes	0.737 (836/1135)	0.878 (462/526)	0.614 (374/609)	0.663	0.878	0.756
JSC Whipple	0.763 (866/1135)	0.844 (444/526)	0.693 (422/609)	0.704	0.844	0.768
JSC Whipple (mod)	0.765 (868/1135)	0.844 (444/526)	0.696 (424/609)	0.706	0.844	0.769

$$\begin{aligned}
 r_{S/D} &= \frac{t_w(t_b = 0)}{t_w\left(t_b / d_p = (t_b / d_p)_{crit}\right)} \\
 &= \frac{0.6 d_p^{19/18} \rho_p^{0.5} (\cos\theta)^{5/3} V^{2/3} (40/\sigma_y)^{1/2}}{0.16 d_p^{1/2} (\rho_p \rho_b)^{1/6} m_p^{1/3} (V \cos\theta) S^{-1/2} (70/\sigma_y)^{1/2}}
 \end{aligned}$$

and $(t_b / d_p)_{crit}$ is given by Eq. (36).

In [37] a database of 1116 hypervelocity impact experiments were compiled, building upon that used for evaluating the JSC Whipple BLE in [10]. We have supplemented that database with data from 19 additional experiments sources from [38]. That database is used to evaluate the

performance of the Whipple shield BLEs presented in this chapter. The results of the evaluation are provided in Fig. 23 and Table 5.

The modified JSC Whipple BLE is shown in Table 5 to provide the best overall performance, with a F1-score of 0.769 (compared to 0.723 for the NNO). The Reimerdes equation correctly predicts more of the perforation test results, i.e., the modified JSC Whipple equation has more non-conservative predictions (false negatives) than the Reimerdes equation: 82 vs. 64. This is because the Reimerdes low velocity form is more conservative than the JSC Whipple, particularly for oblique impacts (see section 7). The additional conservatism is realised in the reduced precision score for the Reimerdes BLE.

8. Application of the Whipple shield BLE

To promote the consistent application of Whipple shield BLEs an open-source Python repository has been created at [11], pyBLOSSUM. The repository includes code for the original NNO, Christiansen-modified NNO, Reimerdes-modified NNO, JSC Whipple, as well as the proposed modifications to the JSC Whipple BLE. In addition, all experimental databases used to evaluate the performance of the different Whipple shield BLEs are provided.

9. Summary and conclusions

Ballistic limit equations (BLEs) are used to design and assess the performance of protective systems for spacecraft subject to impact by micrometeoroid and orbital debris (MMOD) particles at hypervelocity. Due to the typical impact velocities encountered in low Earth orbit (LEO), most spacecraft structures that are designed to provide some level of MMOD protection consist of multiple elements separated by either a void or structural support. For such multi-plate configurations, the outer sacrificial layer (aka bumper) is used to induce fracture, melting, and vaporisation of the impacting MMOD particle, resulting in a less lethal, distributed loading of the spacecraft hull compared to what would be experienced by a single, monolithic structure.

In calculating mission risk to MMOD impact, BLEs must be defined for all structural elements and critical components of a spacecraft. Nearly all such BLEs, for e.g., honeycomb core sandwich panels, foam core sandwich panels, multi-shock shields, toughened thermal blankets, etc., are modifications of Eric Christiansen's so-called new non-optimum (NNO) equation for aluminium Whipple shields. Thus, it is important to understand both the genesis of this equation, and the modifications that have been proposed since its initial publication in 1990.

We have reviewed the original NNO equation as well as the origin of its constituent parts, e.g., hypervelocity cratering relationships in the low velocity regime and the NASA non-optimal Whipple shield equation in the hypervelocity regime, etc. Proposed modifications to the NNO are reviewed and their performance evaluated against experimental databases available at the time of their respective publication. In multiple instances the original published equations included typos, mistakes, or oversights – which we identify and rectify. Finally, a further modification to the JSC Whipple equation is proposed to address issues with discontinuities inherent in the Reimerdes modification to the NNO and the original JSC Whipple BLEs. To enable consistent application of the reviewed equations an open-source repository has been created that includes Python code for each of the equations reviewed in this article, together with experimental databases used for evaluating their performance.

CRediT authorship contribution statement

S Ryan: Writing – review & editing, Writing – original draft, Visualization, Validation, Software, Methodology, Investigation, Formal analysis, Data curation, Conceptualization. **WP Schonberg:** Writing – review & editing.

Declaration of competing interest

The authors declare the following financial interests/personal relationships which may be considered as potential competing interests: An author is an editor for IJIE (William Schonberg) - An author is on the editorial advisory board of IJIE (Shannon Ryan) If there are other authors, they declare that they have no known competing financial interests or personal relationships that could have appeared to influence the work reported in this paper.

Data availability

All data used in the manuscript is provided in the referenced GitHub repository

References

- [1] Whipple FL. Meteorites and space travel. *Astron J (N Y)* 1947;116:1:131.
- [2] Christiansen EL. Meteoroid/Debris shielding. Houston: NASA Johnson Space Center; 2003. NASA TP-2003-210788.
- [3] Madden R. Ballistic limit of double-walled meteoroid bumper systems. Langley Station: NASA Langley Research Center; 1967. NASA TN D-3916.
- [4] Christiansen EL. Whipple shield sizing equations. Houston: NASA Johnson Space Center; 1991. NASA SN3-91-19.
- [5] Maiden CJ, McMillan AR, Sennett RE, Gehring JW. Experimental investigations of simulated meteoroid damage to various spacecraft structures. Santa Barbara: GM Defense Research Laboratories; 1965. NASA CR-65222.
- [6] Cour-Palais B. Meteoroid protection by multiwall structures. Cincinnati: Hypervelocity Impact Conference; 1969.
- [7] A.R. Coronado, M.N. Gibbins, M.A. Wright, P.H. Stern, "Space station integrated wall design and penetration damage control: users guide for design analysis code BUMPER", Boeing Aerospace Company, Seattle, Report D180-30550-2, NASA Contract NAS8-36426, 1987.
- [8] Christiansen EL, Kerr JH. Ballistic limit equations for spacecraft shielding. *Int J Impact Eng* 2001;26:93–104.
- [9] Reimerdes HG, Noelke D, Schaefer FK. Modified Cour-Palais/Christiansen damage equations for double-wall structures. *Int J Impact Eng* 2006;33:645–54.
- [10] Ryan S, Christiansen EL. Micrometeoroid and orbital debris (MMOD) shield ballistic limit analysis program. Houston: NASA Johnson Space Center; 2009. NASA/TM-2009-214789.
- [11] Ryan S. pyBLOSSUM – a Python library for assessing the Ballistic Limit of Spacecraft Structures Under Micrometeoroid and orbital debris impact. GitHub repository 2023-11-08. <https://github.com/shannonjryan/pyBLOSSUM>. accessed.
- [12] Frost VC. Meteoroid damage assessment. Aerospace Corporation; 1970. NASA SP-8042.
- [13] Cour-Palais B. A career in applied physics: Apollo through Space Station. *Int J Impact Eng* 1999;23:137–68.
- [14] Smith RE. Space and planetary environment criteria guidelines for use in space vehicle development. Huntsville: NASA Marshall Space Flight Center; 1971. NASA TM-X-64627.
- [15] M.D. Bjorkman, J.D. Geiger, E.E. Wilhelm, "Space station integrated wall design and penetration damage control: theoretical analysis of penetration mechanics (Task 3)", Boeing Aerospace Company, Seattle, Report D180-30550-3, NASA Contract NAS8-36426, 1987.
- [16] Wilkinson JP. A penetration criterion for dual-walled structures subject to meteoroid impact. *AIAA J* 1969;7(10):1937–43.
- [17] A.R. Coronado, M.N. Gibbins, M.A. Wright, P.H. Stern, "Space station integrated wall design and penetration damage control: final report", Boeing Aerospace Company, Seattle, Report D180-30550-1, NASA Contract NAS8-36426, 1987.
- [18] Cour-Palais B. Hypervelocity impact in metals, glass, and composites. *Int J Impact Eng* 1987;5:221–37.
- [19] Christiansen EL. Design and performance equations for advanced meteoroid and debris shields. *Int J Impact Eng* 1993;14:145–56.
- [20] Christiansen EL. Shield sizing equations. Houston: NASA Johnson Space Center; 1990SN3-90-131.
- [21] Christiansen EL. Shield sizing and response equations. Houston: NASA Johnson Space Center; 1991SN3-91-42.
- [22] Christiansen EL, Arnold J, Davis A, Hyde J, Lear D, Liou J-C, Lyons F, Prior T, Ratliff M, Ryan S, Giovane F, Corsaro B, Studor G. Handbook for designing MMOD protection. Houston: NASA Johnson Space Center; 2009. NASA/TM-2009-214785.
- [23] A.R. McMillan, "Experimental investigations of simulated meteoroid damage to various spacecraft structures", NASA CR-915, 1968.
- [24] Swift HF. Hypervelocity impact mechanics. In: Zukas, editor. *Impact dynamics*. John Wiley & Sons; 1982. editor.
- [25] Alme ML, Rhoades CE. A computational study of projectile melt in impact with typical Whipple shields. *Int J Impact Eng* 1995;17:1–12.
- [26] Cour-Palais BG. Hypervelocity impact investigations and meteoroid shielding experience related to Apollo and Skylab. *Orbital Debris* 1985:247–75.
- [27] Denardo B.P., Summers, J.L., Nysmith, C.R. Projectile size effects on hypervelocity impact craters in aluminum. NASA Ames Research Center, Moffett Field, NASA TN D-4067, 1967.
- [28] Wohlers W, Reimerdes H-G. Analytical optimisation of protection systems. *Int J Impact Eng* 2003;29:803–19.
- [29] Fish RH, Summers JL. The effect of material properties on threshold penetration. In: Proceedings of the Seventh Hypervelocity Impact Symposium; 1965.
- [30] Hayashida KB, Robinson JH. Single wall penetration equations. Huntsville: NASA Marshall Space Flight Center; 1991. NASA TM-103565.
- [31] Piekutowski AJ. Fragmentation-initiation threshold for spheres impacting at hypervelocity. *Int J Impact Eng* 2003;29:563–74.
- [32] Ryan S, Bjorkman M, Christiansen EL. Whipple shield performance in the shatter regime. *Int J Impact Eng* 2011;38:504–10.

- [33] H.-G. Reimerdes, D. Noelke, F.K. Schaefer, "Modified Cours-Palais/Christiansen damage equations for double-wall structures", presented at the hypervelocity impact symposium, Lake Tahoe, 2005.
- [34] Squire MD, Cooke WJ, Williamsen J, Kessler D, Vesely WE, Hull SH, Schonberg W, Paterson GE, Jenkin AB, Cornford SL. Joint polar satellite system (JPSS) micrometeoroid and orbital debris (MMOD) assessment. Hampton: NASA Engineering Safety Center; 2015. NASA/TM-2015-218780.
- [35] Ryan S. Micrometeoroid and Orbital Debris (MMOD) shield ballistic limit analysis program. NASA 2013. MSC-24582-1.
- [36] Schonberg WP, Jenkins AB. Comment on the Reimerdes ballistic limit equation for dual-wall structural systems. *J Spacecr Rockets* 2016;53(3):584–6.
- [37] Ryan S, Sushma NM, Le H, Arun Kumar AV, Berk J, Nguyen TM, Rana S, Kandanaarachchi S, Venkatesh S. The application of machine learning in micrometeoroid and orbital debris impact protection and risk assessment for spacecraft. *Int J Impact Eng* 2023;181:104727.
- [38] Piekutowski AJ, Poorman KL. Effects of scale on the performance of Whipple shields for impact velocities ranging from 7 to 10km/s', proceedings of the 12th hypervelocity impact symposium. *Procedia Eng* 2013;58:642–52.